THESIS/DISSERTATION APPROVED BY

10/19/2010

Date

David Z.Z. He, Ph.D.
Major Advisor

Kirk W. Beisel, Ph.D.

Bernd Fritzsch, Ph.D.

Garrett A. Soukup, Ph.D.

John A. Yee, Ph.D.

Gail M. Jensen, Ph. D., Dean

The Structure-Function Relationship of Prestin:

from an Evolutionary Perspective

by

Xiaodong Tan

A DISSERTATION

Submitted to the Faculty of the Graduate School of Creighton University in

Partial Fulfillment of the Requirements for the Degree of Doctor of

Philosophy in the Department of Biomedical Sciences

Omaha, NE

October 14, 2010

ABSTRACT

Prestin is the motor protein of cochlear outer hair cells. It belongs to a distinct anion transporter family called solute carrier protein 26A, or SLC26A. Members of this family serve two fundamentally distinct functions. While most members transport different anion substrates across a variety of epithelia, prestin (SLC26A5) uniquely functions as a voltage-dependent motor protein. This voltage-dependent response of prestin is accompanied by a charge movement, which is reflected in nonlinear capacitance (NLC). . Prestin is assumed to contain a tunnel-like structure which is only accessible from intracellular side, based on a hypothetical working model as a partial anion transporter proposed by Oliver et al. (2001). Intracellular anions such as Cl^- act as the external voltage sensor of prestin and trigger the conformational change in the molecule, which in turn alters the surface area of plasma membrane. This study tends to gain insight on the functionally critical structures of prestin using comparative approach.

Recent evidence suggests that prestin orthologs from zebrafish and chicken retain transporter function without motile capability. Mammalian prestin does not appear to transport anions across the cell membrane, while controversial studies suggest that mammalian prestin may also be able to transport anions and this transporter function is independent with its electromotility capability. These studies suggest that prestin is evolved from an anion transporter. In this study, I first examined the motor and transport functions of prestin and its orthologs from four different vertebrate species (zebrafish, chicken, platypus and gerbil), to gain insight regarding how these two physiological functions might have distinctly evolved. Somatic motility, voltage-dependent NLC and transporter function were measured in transfected human embryonic kidney (HEK) cells using voltage-clamp and anion uptake techniques. Zebrafish and chicken prestins both

exhibit weak NLC with peaks significantly shifted in the depolarization (right) direction. This is contrasted by robust NLC with left-shifted peaks for both platypus and gerbil prestins. Platypus and gerbil prestins may only retain little transporter function in comparison with robust anion transport capacities in the zebrafish and chicken orthologs. Somatic motility is only detected in the platypus and gerbil prestins. There appears to be an inverse relationship between NLC and anion transport functions, whereas the motor function appears to have only emerged in mammalian prestin. Our results suggest that motor function is an innovation of mammalian prestin and is concurrent with diminished transporter capability.

Evolutionary studies combined with comparative genomic and bioinformatic analyses have identified highly conserved sequences among mammalian prestins that show significant variability among nonmammalian vertebrate prestin orthologs and other SLC26A paralogs. Among these sequences is one segment of 11 residues. In the second part of this study, I investigated whether this region represents the minimal essential motif for the motor function. Chimeric proteins swapping corresponding residues of prestin orthologs from zebrafish and chicken with those from gerbil prestin (zebrafish prestin with gerbil sites, Zf(g), and chicken prestin with gerbil sites, Ck(g), respectively) were constructed. Motility, NLC and anion transport were examined. A gain of motor function was observed with two hallmarks (NLC and motility) in both Zf(g) and Ck(g) without loss of transport function. These results show that the substitution of only 11 amino acids is sufficient to confer motor function upon the electrogenic anion transporters of zebrafish and chicken prestins. Therefore, this segment represents the minimal essential motif for the motor.

The regions or amino acids within prestin that are essential for voltage sensing are still unclear. Charged amino acids are likely to play an important role in voltage sensing because of their potential capability to serve as anion binding sites. Previous studies focused mostly on the property of charged side chains. In the third part of this study, the roles of three positively charged amino acids in voltage sensing of prestin were examined. I hypothesize that the size or charge location of the amino acid side chain is also an important factor for prestin function. Three positive amino acids in the putative tunnel region were selected based on molecular dynamics simulation and sequence alignment of prestin paralogs and orthologs, namely R197, K227 and K449. A series of substitutions using similarly charged amino acids (R to K and K to R) are constructed, assuming that R and K substitutions only affect size and charge orientation of the side chain. Negative (R / K to E), neutral (R / K to A) substitutions and combinations of substitutions at these three sites (double and triple mutations) were also constructed assuming that there are multiple anion binding sites in the molecule. The results show that all three sites are important for voltage sensing and that the size or charge orientation of the side chain is also a critical factor. Furthermore, negative correlations between the peak voltage of NLC or the total charge movement and the slope factor are observed, suggesting that other electrical features such as dielectric properties were changed by these substitutions rather than the number of charges or their traveling distance.

ACKNOWLEDGEMENTS

Three years' experience in the Graduate Program of Creighton University is delightful and fruitful for me, because of the interesting project I have been taking and all the nice people I met in and beyond my academic study. My thanks go to all my advisors, co-workers and other friends, who gave me their unselfish guidance, constructive suggestion, generous support and warm friendship.

I am greatly indebted to my major advisor Dr. David He, Professor of the Department of Biomedical Sciences, for providing me the opportunity to continue my scientific career in the United States, for the much guidance and encouragement throughout my study, and for the understanding and supporting during my hard times. He also served as a good example of outstanding and dedicate scientist to me. I am also very much obliged to Dr. Kirk Beisel, also the Professor of the Department of Biomedical Sciences, for his remarkable insight and tremendous dedication in this project, and for his enormous help on my graduate study and my future career development. The realization of the thesis would not have been made possible without the original ideas from them and the cooperation of their two laboratories.

My sincere appreciation is also due to all other members of my advisory committee. To Dr. Garrett Soukup, for his kindness of allowing me to work in his laboratory, and for his generous instructions to me on both the scientific idea and technology. To Dr. John Yee, the chairman of our department, for his thoughtful vision on my project and his kind recommendation for my post doctorate position. To Dr. Bernd Fritzsch, the chairman of Department of Biology in University of Iowa, for his advices and contributions on each and every stage of my project.

My thanks also go to other laboratories and facilities in Creighton. These include Dr. Soukup's laboratory, Dr. Sandor Lovas' laboratory and the Integrated Biomedical Imaging Facility in Biomedical Department, Dr. Zhao-Yi Wang's laboratory and Dr. Xianming Chen's laboratory in Department of Medical Microbiology and Immunology, and Dr. Perry Greg in Flow Cytometry Core Facility. I got enormous assistances and suggestions from them.

I would also like to convey my gratefulness to all my co-workers. Thanks to Mr. Jason Pecka in Dr. Beisel's laboratory, who taught me hand by hand all kinds of techniques on molecular biology and helped by constructing all the plasmids I need in the project. Thanks to Mrs. Shuping Jia in our laboratory, who helped me with the experimental skills and kept the running of our laboratory. Thanks to Dr. Jie Tang, the post doctorate of our laboratory, who helped me collecting the data and solving technical and academic problems. Thanks to Dr. Qian Zhang, PhD student in our department, who helped me both in experimental operations and in everyday life by taking care of my family.

Special thanks to other professors and other peer colleagues in our department, who helped me with my course studies, experiments, research project, thesis writing, etc. This includes but not limited to: Dr. Laura Hansen, Dr. Richard Hallworth, Heather Smith, Zhifei Shao, Jun Liu, Rui Zhou, Marsha Pierce, Benjamin Currall, Alicia Bryan and Kyle Bichsel. It is them who made my journey more enjoyable and informative.

My deepest gratitude is attributed to my family, my wife Dr. Yingjie Zhou and son Ruiyang Tan. They are the essential spiritual support and motivation which inspired me to fulfill the program in Creighton and achieve my next goal.

TABLE OF CONTENTS

ABREVIATIONS

CHO	Chinese hamster ovary
DIDS	4,4’-diisothiocyanatostilbene-2,2’-disulfonic acid
EL2	External loop 2
HEK	Human embryonic kidney
IHC	Inner hair cells
meEM	Minimum essential electromotility motor
MET	Mechano-electrical transduction
NLC	Non-linear capacitance
NMV	Nonmammalian vertebrates
OHC	Outer hair cells
PAT	Partial anion transporter
SLC26A	Solute carrier 26A gene family
SulpTP	Sulfate transporter
TMD	Transmembrane domain
gPres	Gerbil prestin
pPres	Platypus prestin
cPres	Chicken prestin
zPres	Zebrafish prestin
Zf(g)	Zebrafish prestin with gerbil meEM motif
Ck(g)	Chicken prestin with gerbil meEM motif
α	Slope factor of the voltage dependence of charge transfer
C_{lin}	Linear capacitance
Q_{max}	Maximum charge movement
$V_{1/2}$	Peak voltage of the nonlinear capacitance
z	Valence of charge movement

LIST OF TABLES

LIST OF FIGURES

CHAPTER 1: BACKGROUD AND LITERATURE REVIEW

I. MAMMALIAN COCHLEAR AMPLIFICATION: TWO PUTATIVE MECHANISMS

A. The mammalian cochlea: anatomy and physiology

The mammalian inner ear is a complex system embedded deep in the temporal bone. Two functional components co-locate in this labyrinthine structure. The first is the vestibular and semicircular canals, which are in charge of the sensation of balance and posture. The other is the cochlea, which is the auditory organ (Fig. 1-1*A*). The cochlea is a coiled duct filled with fluid and is divided into three scalae: scala vestibuli, scala media and scala tympani. The scala vestibuli and the scala tympani are joined at the apex of the cochlea and filled with high Na^+ perilymph, while the scala media is a single continuous occluded compartment filled with high K^+ endolymph that is higher in potential than perilymph (+80 mV). The basilar membrane, on which the Organ of Corti is located, is the partition between the scala media and the scala tympani. The Organ of Corti is a highly specialized structure containing hair cells and their supporting cells. Hair cells are mechanosensory cells. Morphologically, actin-rich stereocilia that protrude from the apical surface of hair cells are organized in staircase-like rows of increasing heights. Neighboring taller and shorter stereocilia are connected by tip links stretching out from the tips of shorter ones and ending on the lateral of taller ones, right where the mechano-electrical transduction (MET) channels reside. This well-organized hair bundle is overlaid by a gelatinous flap, the tectorial membrane, and the tips of the hair bundle are stuck into the tectorial membrane, forming a mechanically coupled unit. The hair cells can be divided into two categories, the inner hair cells (IHC) and outer hair cells (OHC), separated by pillar cells. Typically the mammalian Organ of Corti has one row of IHC and 3 rows OHC are arranged along the basilar membrane (Ashmore 2008; Pickles 2008).

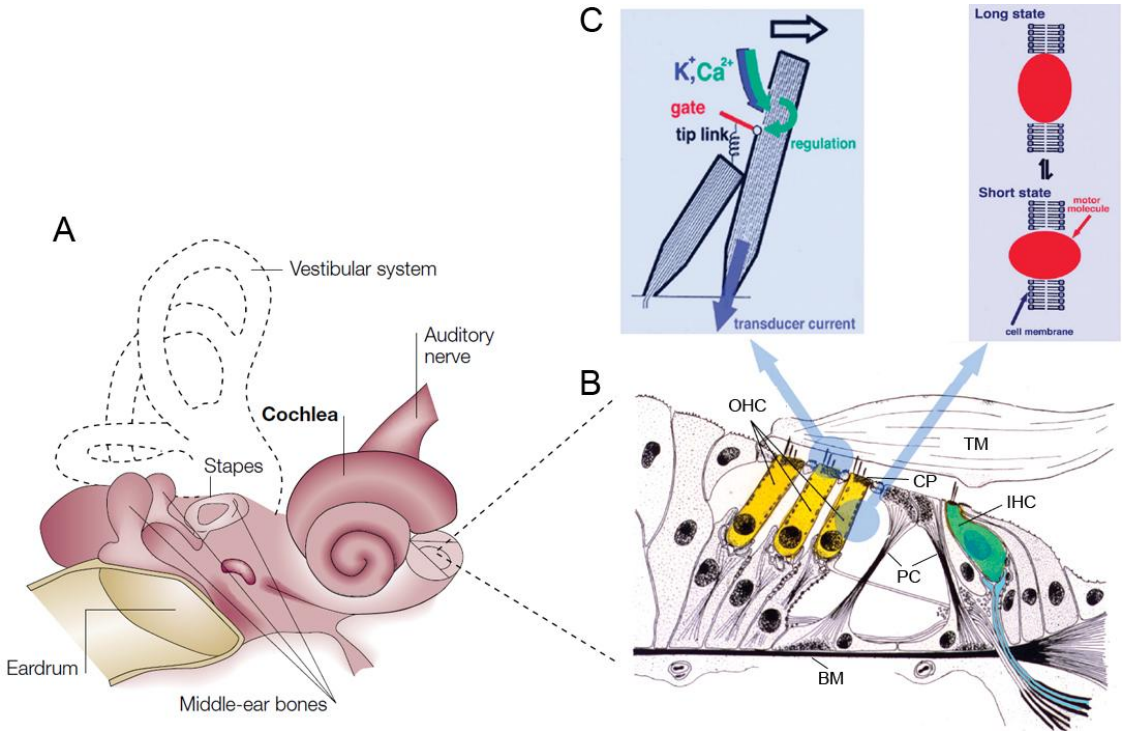

Figure 1-1. ***A.*** Schematic structure of inner ear showing the relative positions of the vestibular system and the cochlea, the organs responsible for the sensation of balance and hearing, respectively. ***B.*** Cross-section of the cochlea showing the structure and basic components of the Organ of Corti. One row of IHC and three rows of OHC are separated by the pillar cells, different in both morphology and function. Hair cells are embedded in basilar membrane with the stereocilia protrude from the cuticular plate. Other supporting cells help connect hair cells to the basilar membrane. The tectorial membrane is an acellular gelatinous structure loading on the surface of the basilar membrane. OHC: outer hair cells; IHC: inner hair cell; TM: tectorial membrane; CP: cuticular plate; PC: pillar cells; BM: basilar membrane. ***C.*** Two putative mechanisms of the mammalian cochlear amplification process. Left: the MET channel-based stereocilia movement. Right: prestin-based somatic motility. See the text for more details (*modified from (Dallos and Fakler 2002) and (Dallos 2008)*).

The function of the cochlea is to convert the mechanical signal of sound into the electrical signal which can be decoded and analyzed by the auditory system. The tectorial membrane, organ of Corti and basilar membrane constitute the mechanical structure for

this conversion and hair cells are responsible for this mechano-electrical transduction (Ashmore 2008). The high potential differences between the perilymph and endolymph (80 mV), together with the membrane potential of the hair cells (60 mV), supply the power for this process (Davis 1965; Davis et al. 1958).

The cochlea in nonmammalian vertebrates (NMV) is a papilla rather than a coiled structure, with less distinctive hair cells. Despite similarities in their vestibular system, the auditory part of the inner ear in lower vertebrates is quite different from that of mammals. Although different hair cell types are observed in reptiles and birds, the transition of different types is gradual in the basilar papilla, unlike the clear-cut dichotomy of the IHC and OHC in mammalian inner ear. Furthermore, the coverage of the tectorial membrane is often incomplete in nonmammalian species (Manley 2000).

B. Cochlear amplification: physics and cellular origin

The cochlea works as a frequency analyzer of the acoustic signal. Sound waves from outside environment are transmitted into the cochlea and travel along the basilar membrane in the fluid-filled cochlea duct. The vibration of the basilar membrane increases in amplitude until reaching a maximum at a location intimately related to the frequency of the incoming sound. In this way, the acoustic signal is decomposed into its component frequencies and picked up at different locations on the basilar membrane along the longitudinal axis of the cochlea duct. This working mechanism of the cochlea known as the “Traveling-Wave Theory” was proposed by Bekesy (1960). Accordingly, a highly ordered tonotopic organization is observed on basilar membrane, with high frequencies detected in the basal and low frequencies in the apical region of the cochlea (Bekesy 1960). However, irreconcilable discrepancy between the living cochlea and the physical frequency analyzer remains, since the sensitivity and frequency tuning of the

living cochlea is much more sensitive and sharp than dead ones. Because this exquisite frequency selectivity and sensitivity cannot be explained solely by the passive process of the mechanical system, a theory of an active amplification mechanism in the inner ear has been proposed (Gold 1948; Gold and Pumphrey 1948). According to this theory, extra energy generated through positive feedback is put back into the system to enhance the input signal and tuning of frequency. Direct evidence for the existence of the otoacoustic emission which represents the energy generation process in the inner ear was reported in 1978 (Kemp 1978). This so called "cochlear amplifier" is responsible for a gain of 40-60 dB (i.e. 100-1000 times), especially at low sound level (Ashmore 2008; Dallos and Fakler 2002; Robles and Ruggero 2001; Sellick et al. 1982). An equivalent active inner ear amplification process also exists in NMV (Hudspeth 2008; Manley et al. 2001).

C. Stereocilia movement: the energy source of inner ear amplification of NMV

The generator of the cochlea amplifier is located in the mechanical structure of the inner ear and has in effect been proven to be the ciliated hair cells (Fig. 1-1*B*). In NMV, sound waves cause the relative movement of the cuticular plate of the hair cells and tectorial membrane, generating shear force that deflects the hair bundle. The deflection of stereocilia toward the taller ones opens the MET channel on the lateral wall of stereocilia via the tip link. The MET channels are permeable to potassium and calcium ions. The opening of the channels generates inward currents driven by the potential difference of some 140 mV, due to the ion environments in the endolymph and the summation of the endocochlear potential and the cell's resting potential. The potassium current is dominant and generates receptor potential. The influx of calcium regulates the slow and fast adaptation of the channels. Fast adaptation controls the channel open probability and produces active hair bundle motion, which serves as the energy source for the cochlear

amplification (Holt and Corey 2000; Hudspeth et al. 2000; Ricci et al. 1998). In other words, the opening and closing of the MET channels generate force which is transmitted back into the hair bundle to reinforce its vibration. This amplification mechanism is proven by the observations of the active mechanical reaction on hair bundles of NMV hair cells and its spontaneous movements (Crawford and Fettiplace 1985; Hudspeth 1997; Hudspeth et al. 2000).

D. OHC electromotility: mechanism of mammalian cochlear amplification

In the mammalian cochlea, things are more complicated because of its more delicate structural and functional features. The mammalian cochlea is characterized by dichotomy of its hair cells, distinct in their spatial locations, morphology and functions (Fig.1-1*B*). IHC serve as the mechano-electrical transducer for the conversion of the mechanical vibration into an electrical signal. OHC, on the other hand, may have lost the capability of signal transduction while specialized as voltage driven motor cells (Fig. 1-1*C*). OHC can rapidly change their somatic length when the potential across the cell membrane changes: depolarization leads to contraction of the cell while hyperpolarization leads to elongation (Brownell et al. 1985). In this way OHC may provide a voltage-dependent force to the vibration of the basilar membrane that enhances the mechanical input to IHC and thus reinforces the tuning and amplification of the system. This so-called "electromotility" of OHC was first reported by Brownell et al. (1985) and has been observed in all the animals studied including mice (Abe et al. 2007), rats (Belyantseva et al. 2000), gerbils (He et al. 1994), guinea pigs (Brownell et al. 1985; Navarrete and Santos-Sacchi 2006). The electromotility motor is located on the lateral membrane of OHC (Iwasa 1994; Kalinec et al. 1992). Electromotility in OHC is a piezoelectric phenomenon (Dong et al. 2002; Gale and Ashmore 1994; Iwasa 2001; Ludwig et al.

2001), which means that mechanical loading of these cells may cause the increase of electrical impedance and extend the frequency bandwidth of the cells' response. The electromotility of OHC provides an alternative source of power for the mammalian cochlear amplifier.

The dominant energy source for mammalian cochlea amplification may still come from hair bundle motion of OHC because it seems unnecessary to evolve two different mechanisms to achieve the same function. It is proposed that the role of OHC somatic motility is just to set the operating point of stereocilia by adjusting their position (Chan and Hudspeth 2005; Kim 1986; Russell et al. 1986), while this is not supported by the evidence acquired from a knock-in mouse model (Gao et al. 2007). Nevertheless, the spontaneous movement of stereocilia, which is thought to be one of the hallmarks of the active process (Hudspeth 1997; Hudspeth 2008), was recently observed in mammalian OHC, with a mechanical force of over 500 pN (Kennedy et al. 2005; Kennedy et al. 2003). This is the most convincing evidence of the role of hair bundle motion in mammalian cochlear amplification to date.

Controversies as to which one of the two mechanisms dominates mammalian cochlear amplification arose right after the discovery of OHC electromotility. Proponents of somatic motility believe the highly specific structure of mammalian cochlea and newly-developed amplification mechanism underpins the outstanding performance of mammalian hearing, the more extended frequency range and sophisticated frequency and intensity discrimination. Supporting observations include that, in the absence of OHC, the hearing sensitivity is severely damaged and frequency discrimination is also compromised. Furthermore, to participate in acoustic tuning, the movement of OHC should be fast enough to accommodate the frequency range of mammalian hearing, as

high as nearly 100 kHz in some species. Precise measurements using fast response photodiodes showed that the frequency of the length change of OHC could reach up to 70 KHz, while the speed of OHC motility measurements is often limited by the recording technologies (Dallos and Evans 1995; Frank et al. 1999; Gale and Ashmore 1997). More convincing studies on knock-out (Liberman et al. 2002) and knock-in (Dallos et al. 2008) mice have validated the role of somatic motility of OHC in cochlear amplification. On the other hand, the force generated by OHC stereocilia is too small to account for the mass energy of the cochlear amplifier (Xue et al. 1995) compare to that of the somatic motility, which is several times to the mass of OHC itself.

Somatic motility of OHC is more widely accepted as the force powering mammalian cochlear amplifier, but the debate is currently unsolved. The two putative mechanisms are schematically illustrated in Fig. 1-1C. Considering that the hair bundle motion and somatic motility of OHC are coupled in the Organ of Corti (Jia and He 2005), it is plausible that they both contribute to the amplification.

II. PRESTIN: THE MOLECULAR BASIS OF OHC MOTILITY

A. Identification of the motor of OHC: prestin molecule and OHC membrane particles

As a notation of its motile function, the OHC are cylindrical cells whose length change is mainly along its longitudinal axis. These characteristic shape and force generating axis are mostly due to the specific cytoskeleton of OHC lateral wall. Another morphological feature of OHC is the dense particles in the lateral wall which occupies about 75% of the surface area of the lateral membrane (He et al. 2010; Zheng et al. 2000). When examined in freeze fracture, these densely packed particles have exhibited a diameter of about 11 nm (Gulley and Reese 1977). It was proposed that a unique motor protein may be

embedded in the OHC plasma membrane (Kalinec et al. 1992), and the molecular nature of this motor was revealed by Zheng and colleagues (Zheng et al. 2000). A subtractive gene cloning strategy was used based on the fact that IHC did not show somatic motility but shared many similarities with OHC. The OHC-IHC subtracted cDNA library was established to identify OHC-specific genes and one of the prevalent genes was the membrane-located motor protein of OHC, named prestin. Amino acid sequence and gene structure analysis indentify prestin to be the fifth member of an anion transporter family called solute carrier protein 26A, or SLC26A (Zheng et al. 2002). It has 744 amino acids consisting 10 to 12 membrane-spanning helices (Deak et al. 2005; Oliver et al. 2001; Rajagopalan et al. 2006; Santos-Sacchi et al. 2001; Zheng et al. 2001).

Several convincing studies show that prestin is the motor of OHC. Prestin molecules are located in the membrane where the motor is known to be located (Hallworth et al. 1993; Huang and Santos-Sacchi 1993; 1994) and confer both NLC and electromotility to heterogeneously prestin-expressing cells (Zheng et al. 2000). Prestin knock-out mice have shortened OHC with no particles in their lateral membrane and lack motility. This knock-out mice exhibit a hearing loss as great as 40-60 dB (Liberman et al. 2002). Interestingly, this is equivalent to the increment of the cochlear amplification. Recently, prestin knock-in mice in which the prestin is immobilized by mutations of V499G and Y501H, showed a 40-60 dB hearing lost without any changes on the morphology of the cells or the cytoachitecture of the cochlea (Dallos et al. 2008). This observation provides indisputable evidence that the motility of OHC, based on its motor molecule prestin, is the energy source of cochlea amplifier. Nevertheless, 744 amino acids of prestin protein cannot account for the 11 nm particles on the observed OHC membrane. Taking this into account, prestin molecules are believed to polymerize into a homomultimeric protein

(Ashmore 2008; Zheng et al. 2006) although each of the subunits may function independently (Wang et al. 2010).

B. Functional features of prestin: Motility and NLC, the two hallmarks

The electromotility of prestin is totally different from the movement of other motor proteins. First, prestin is embedded in membrane instead of moving along tracks such as microtubules (Kalinec et al. 1992). Second, the motility of prestin is a voltage-driven process and is ATP and Ca^{2+} independent, which means it does not require energy (Holley and Ashmore 1988). Third, the movement of prestin is piezoelectric-like and extremely fast (Ludwig et al. 2001). These unique properties indicate that prestin undergoes a different mechanism and speed beyond any known contractile pattern.

Another remarkable character of prestin is the nonlinear capacitance (NLC) that accompanies its mechanical response. This property results from charge movement inside the prestin molecule under the influence of membrane potential. It is a voltage-dependent process similar to the gating current of voltage-gated ion channels. When plotted over voltage, NLC is a bell-shaped curve and is perfectly correlated with the sigmoidal response of the motility: both can be fitted with the two-state Boltzmann function and share indistinguishable fit parameters; inhibition of NLC inextricably leads to the block of the mechanical response. Therefore, NLC is thought to be the electrical signature of motility, and presumably related to the activity of the voltage sensor in the electrical field. Because measuring NLC is easier and more accurate than measuring the motility, it is often used to characterize motility.

C. Structure and function relationship of prestin

Although the amino acid sequence and membrane topology of prestin was identified almost a decade ago, its crystal structure is still missing. A preliminary electron

microscopy study indicated prestin to be in a bullet shape, with a large cytoplasmic domain, while the details of its spatial configuration remain obscure. Nonetheless, it is generally accepted that prestin can be structurally divided into three domains: Amino (N-) terminus, hydrophobic core and carboxyl (C-) terminus (Zheng et al. 2001; Zheng et al. 2000), with the N- and C- termini both in cytoplasm. A sulfate transporter signature motif defining the family is in the second membrane-spanning helix. A sulfate transporter and anti-sigma factor antagonist (STAS) motif, as well as a positively charged cluster and a negatively charged cluster is located in the C-terminus.

Two functional regions of prestin are assumed base on its two essential electrophysiological properties: 1) the voltage sensor region that detects changes in transmembrane potential of the cell, and 2) the actuator region that undergoes a conformational change that produces somatic motility (Dallos and Fakler 2002). Critical sites, functional motifs and regions thought to be important for the functions of prestin have been studied intensely. Substitutions of amino acids, N-, C- termini swapping and truncations base on bioinformatic studies are most commonly used. Changes in NLC properties are most commonly observed alterations in electrophysiology. In addition, the loss of NLC due to the failure of membrane-associated expression is often observed. These studies suggest that the entire or certain areas of the hydrophobic core, N- and C-termini are important for specific function or other molecular characteristics such as proper protein folding, assembly into cytoplasmic vesicles, transportation to the membrane and homo-oligomerization (Kumano et al. 2009; Navaratnam et al. 2005; Pasqualetto et al.; Zheng et al. 2005).

D. Working Mechanism of Prestin: the PAT Model

Prestin shares an overall structure and specific domains with the SLC26A protein family: a highly conserved central core of hydrophobic amino acids predicted to form 10-12 transmembrane domains (TMD) which are assumed to form a tunnel-like structure (Deak et al. 2005; Oliver et al. 2001; Rajagopalan et al. 2006; Santos-Sacchi et al. 2001; Zheng et al. 2001). This tunnel is accessible only from intracellular side and is the structural basis of the partial anion transporter (PAT) model, the simplest working hypothesis of prestin [Fig. 1-2] (Dallos and Fakler 2002). Base on this model, intracellular Cl^- enters and binds to a site within the tunnel and triggers a conformational change in prestin. The anion moves toward the extracellular surface upon hyperpolarization and toward cytoplasmic side in response to depolarization. The charge movement arises from the intracellular Cl^- moving part way through the membrane, and Cl^- is thought to serve as the extrinsic voltage sensor for the voltage driven conformational change (Dallos and Fakler 2002; Oliver et al. 2001). An alternative model in which prestin has its own intrinsic voltage sensor has also been proposed (Bai et al. 2009; Rybalchenko and Santos-Sacchi 2008). In this model chloride is thought to serve as an allosteric modulation by binding to specific sites. In either model, positively charged amino acids in the tunnel region are believed to play an important role in voltage sensing, possibly by serving as the binding sites of the anions during this process.

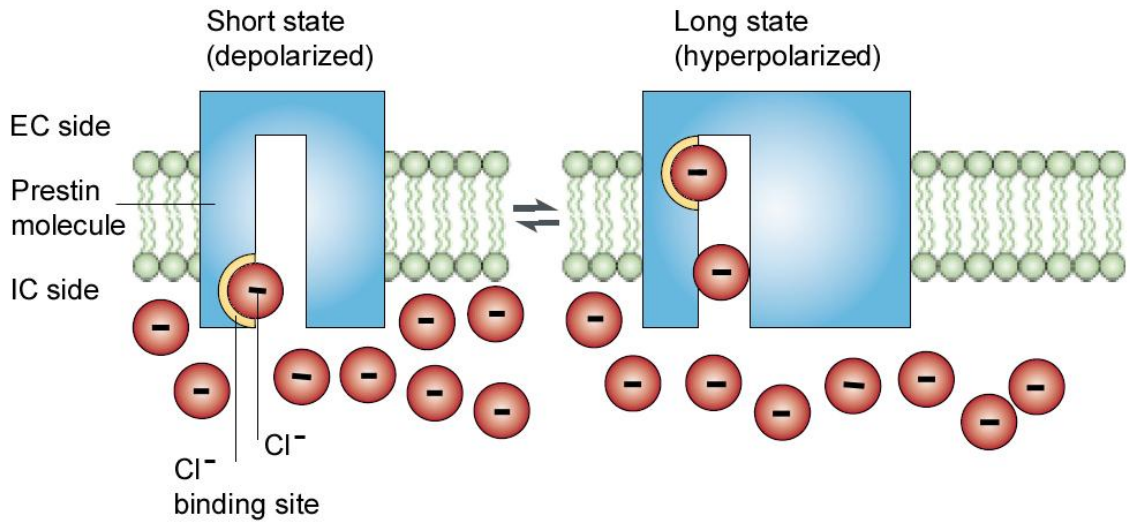

Figure 1-2. The PAT model of prestin. Prestin is assumed to have a tunnel-like structure capable of a two-state conformation. The molecule remains in its short structural state when the cell membrane is depolarized. When the membrane is hyperpolarized, the chloride ions move into the molecule and trigger the conformational change of the molecule to its long state. EC: extracellular; IC: intracellular. (*modified from (Dallos and Fakler 2002)*)

III. EVOLUTIONARY VIEW OF PRESTIN: TRANSPORTER AND/OR MOTOR?

A. Clues from SLC26A family: different function and incompatibility with similar structural features

The SLC26A transporter family consists of eleven members, with SLC26A10 likely to be a pseudogene. All members of this family except prestin are anion exchangers/ channels capable of transporting a wide variety of monovalent and divalent anions (Mount and Romero 2004). By contrast, prestin (SLC26A5) performs rapid electromechanical and mechanoelectrical conversions on a microsecond time scale in OHC (Dallos and Fakler 2002; He et al. 2006). Although all SLC26A members share a highly conserved sulfate transporter signature in the hydrophobic core, the similarity of the whole sequence between individual members is low [21-43% identity] (Dorwart et al.

2008), and the C-terminus is the least conserved region in the whole family. Nonetheless, the transporter function of SLC26A members can be categorized into 3 groups based on their ionic specificity and mode of transport. Members of group 1 are selective sulfate transporters represented by A1 and A2. Members of group 2 are coupled Cl-/HCO3- exchangers and encompass paralogs A3, A4, A6 and A8. Members in this group such as A4 (pendrin) and A6 have the highest sequence homology with prestin. Pendrin (A4) and prestin (A5) are evolved from a common ancestor. Members of group 3 are ion channels, including A7 and A9. The transport mode of A11 is unknown, and SLC26A5 is not included in this taxonomy because it does not appear to function as anion transporter in mammals. However, recent evidence suggests that prestin may transport anions (Bai et al. 2009) as well as provide electrogenic transport of bicarbonate and chloride (Muallem and Ashmore 2006). Data from Bai et al (2009) suggest that the anion transport and electromotility properties of prestin are independent of each other (Bai et al. 2009).

A series of studies based on the comparison of prestin and its paralogs performed by different groups have shown some similarities as well as differences on prestin structure and function. Substituting the N- or C-terminus of prestin with the analogous portion of pendrin (SLC26A4) or PAT1 (SLC26A6), the two closest relatives of prestin, resulted in membrane-expression problems or loss of its electrophysiological function (Navaratnam et al. 2005; Zheng et al. 2005). Failure of membrane-targeting may suggest misfolding of the protein, which has been observed in other studies as well as disease-related mutations of SLC26A family (Dossena et al. 2009; Everett et al. 1997; Hastbacka et al. 1992; Hoglund et al. 1996; Schweinfest et al. 1993). Charged residues in the whole prestin sequence which are unconserved between A5 and A6 were neutralized based on the assumption that the voltage sensing of prestin may involve these novel sites (Oliver et al.

2001). Neither cations nor external anions had any effect on NLC in this study. These results lead to the conclusion that Cl^- ions serve as extrinsic voltage sensor of prestin. By contrast, the results of a second study in which all the conserved charged residues were neutralized suggest an intrinsic voltage-sensing mechanism because of their NLC properties were altered (Bai et al. 2009).

B. Clues from NMV orthologs: functional evolution of prestin

Through comparative genomic, bioinformatic, molecular and expression analyses, prestin orthologs have been identified in the hearing organ mechanosensory cells of insects, zebrafish (*Danio rerio, Dreri*) , and chicken (*Gallus gallus, Ggall*) (Albert et al. 2007; Franchini and Elgoyhen 2006; Rajagopalan et al. 2006; Schaechinger and Oliver 2007; Weber et al. 2003). Physiological evidence suggests that prestin orthologs from zebrafish and chicken are electrogenic divalent/chloride anion exchangers (Schaechinger and Oliver 2007) with no motor function (Albert et al. 2007; He et al. 2003). Moreover, while mammalian prestin orthologs display an extremely high amino acid conservation (92.7% identical among gerbil, mouse, rat and human), they share similar hydrophobicity with its orthologs from zebrafish and chicken. Thus prestin orthologs from mammals and NMV may assume a similar structure (Albert et al. 2007; Schaechinger and Oliver 2007). These studies, together with the fact that prestin belongs to the SLC26A family, suggest that prestin is evolved from an anion transporter.

Base on the bioinformatic studies, the amalgamation of comparative genomic, evolutionary, and structural diversification approaches turns out to be powerful methods in studying prestin structure and function. Comparative genomic analyses revealed detailed sequence conservation among NMV and mammalian SLC26A5. NMV SLC26A5 peptides have a higher degree of sequence variability within the sulfate

transporter and STAS domains, while mammalian SLC26A5 members differ with the high conservation, being in the variations mainly restricted in N- and C- termini (He et al. 2006; Okoruwa et al. 2008). Recently, the comparison of prestin paralogs and orthologs from fish, amphibian, bird, prototherian and eutherian mammals, revealed highly conserved amino acids in mammalian prestin TMD were identified (Okoruwa et al. 2008). Since these conserved sites or motifs distribute over the whole TMD and are unique to mammalian prestin, it was assumed that they contained elements essential for its newly derived motor function of mammalian prestin. Prestin orthologs from prototherian species, such as platypus (*Ornithorhynchus anatinus, Oanat*), that were identified and sequenced (Okoruwa et al. 2008), showed the same sequence conservation in the hydrophobic transporter domain as other mammals. Orthologs from the prototherian and metatherian species are considered evolutionary links with the eutherians that may offer necessary peptide sequence and structural implications of how mammalian prestin electromotility function evolved from the NMV transporter.

C. Clues from the Structure of Other Transporter families: Common structure with no sequence similarity

Although the crystal structure of prestin and other members of the SLC26A family is still unknown, more and more publications on the structure of other transporter families have revealed some common structural features. Although they may have different substrate specificities and no primary sequence similarity, transporters from different families have similarities on their spatial configurations (Diallinas 2008; Faham et al. 2008; Singh et al. 2008; Weyand et al. 2008; Yamashita et al. 2005). This structural similarity implies that transporters may also share a similar or common working mechanism. Recent crystallography data suggest that transporters may utilize a common

mechanism of substrate transport, defined as a rocker-switch model [Fig. 1-3] (Diallinas 2008; Faham et al. 2008; Singh et al. 2008; Weyand et al. 2008; Yamashita et al. 2005). In this model, the ubiquitous structure of transporters contains an inner motile unit including two gates and a central pore which is surrounded by an outer shell. The two gating areas allow the alternative access from the extra- or intracellular sides, while the central pore contains primary substrate binding sites. Secondary binding sites may also exist along the path outside the central pore. The inner motile unit conducts the transportation of ions via the alternative opening and close of the two gates, which are molecular conformational changes induced by the binding of the substrates. This conformational change is able to occur at a turnover rate up to 10^5 per second – at 10 time faster rate of the higher limitation of mammalian hearing frequency (Accardi et al. 2004; Walden et al. 2007).

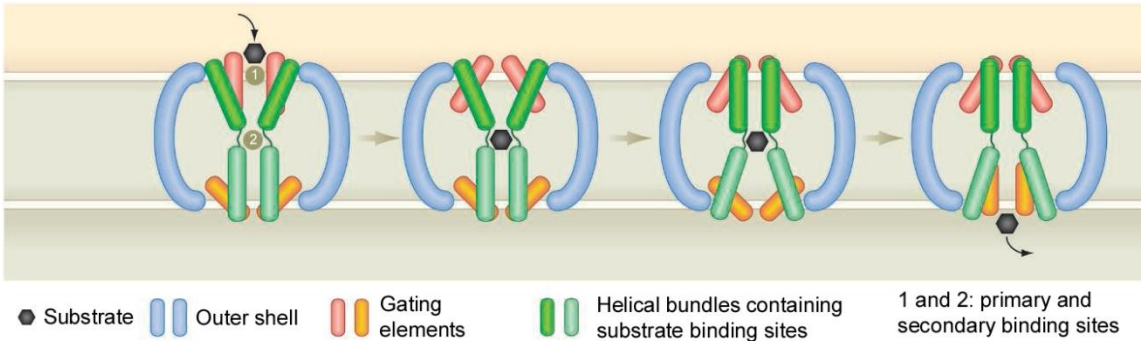

Figure 1-3. Schematic illustration of the gated rocker-switch transporter model and each stage of its conformation. This model is based on crystal structures of several transporters from evolutionary distinct protein families with no sequence similarity (Diallinas 2008; Faham et al. 2008; Singh et al. 2008; Weyand et al. 2008; Yamashita et al. 2005). All of the transporters share a similar structure: an inner core that consists of two gates and a central pore is surrounded by an outer shell. Residues in the gating elements and pore region serve as substrate or ion binding sites. The two gating elements are flexible helices and are the motile units of the

molecule. Helical bundles composing the central pore contain substrate binding sites (primary and sometimes secondary). Substrate binding induces a conformational change in the two gates which allows alternative access of the extra- (the left-most panel) or intracellular (the right-most panel) space. (*modified from (Diallinas 2008)*)

One such model of the rocker-switch mechanism is based on studies of the ClC-ec1, a member of another Cl^- channel/transporter family found in *E. Coli*. The size of the side chain of the amino acids is a more important factor for ion gating than the charge of the amino acids (Jayaram et al. 2008). A mutant ClC-ec1 in which the amino acids in both gates (glutamate and tyrosine, respectively) were mutated to alanine abolished resulted in disruption of both the external and internal gates of the protein. Thus, the transporter was turned into a channel-like protein in the mutated construct.

IV. HYPOTHESIS AND SPECIFIC AIMS

Recently, substantial progress was made regarding the structure and function of prestin, while details of its three-dimensional structure and critical functional domains are still obscure. Important information can be inferred from previous works, including bioinformatic analysis and modeling studies. First, the reciprocity of the piezoelectric property of prestin resembles the transporter function of its NMV ancestors and other family members. In addition, prestin also shares similar membrane topology with its NMV orthologs (Albert et al. 2007). These connections imply a relationship between the evolution of transporter and motility functions. Studies on platypus prestin may offer important insights. Second, motor function of prestin is a newly derived feature in mammals, while the conformational change of its inner core can be speculated as being

an intrinsic property of transporters in general. How this interior movement of substrate transfer may be the key component during the evolution of the motor protein. Third, ion gating/voltage sensing is not only related to the residues serving as the binding sites of the anions, but also determined by contribution of the residue to the site itself. Reconsideration of the mechanisms underlying the voltage sensing of prestin may benefit from these new discoveries.

Specific Aim 1: To determine how prestin evolves from an anion transporter in NMV to a distinct motor protein in mammals. I hypothesize that prestin orthologs in low vertebrates serve as an anion transporter/exchanger with no motor function, while prestin acquires new structures (motifs) and thus gains motor capability and associated with diminished transporter function. To address this, transporter function, NLC and somatic motility of prestin orthologs from gerbil, platypus, chick and zebrafish expressed in a heterologous cell system will be measured, analyzed and compared.

Specific Aim 2: To determine the role of a putative motor region on the motility function of prestin. The putative motor region of prestin molecule is indicated by previous bioinformatic studies (Fig. 1-4). It is unique to mammalian prestin orthologs while highly variable among NMV species. I hypothesize that innovations on this motif confer prestin with its motility function. The association of this region with the transporter and motility functions will be examined. Series mutagenetic studies on chimera proteins swapping this region among different species (gerbil, chicken and zebrafish) will be carried out.

Specific Aim 3: To examine the role of three positively charged amino acids (R197, K227 and K449) in the predicted TMD for voltage sensing. These three sites were identified by bioinformatic studies and structural analyses and assumed to be in the

tunnel region based on their putative locations in α-helical hydrophobic TMD (Fig. 1-4). Arg (R) and Lys (K) are both positive residues and presumably only slightly different in size or charge location of the side chain. I hypothesize that the size or the charge location of these residues is critical for prestin function. Replacement of these residues with each another in these three selected sites may cause major changes in the NLC properties of prestin. Site specific mutagenesis will be used to generate the mutant prestin. NLC, transporter function and somatic motility will again be measured and studied.

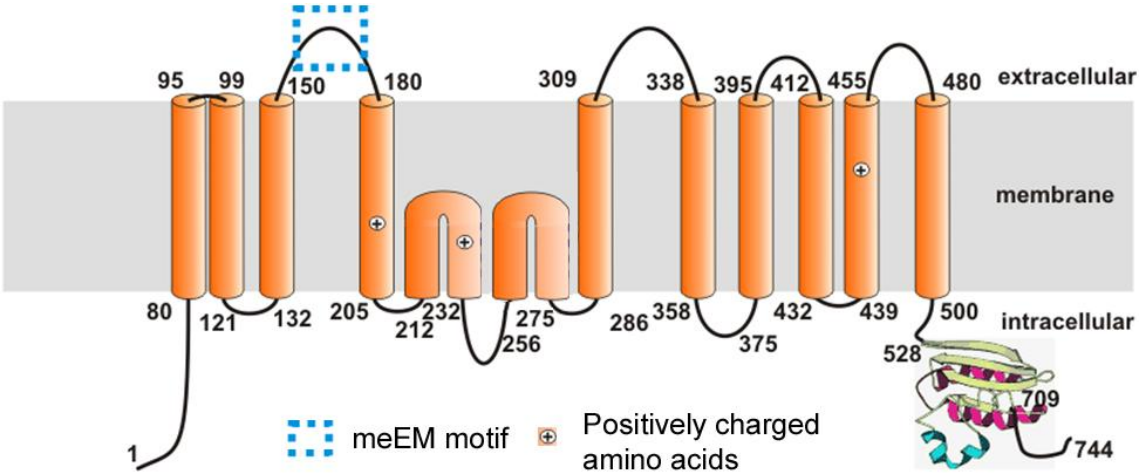

Figure 1-4. A schematic model of the membrane topology of mammalian prestin showing the putative motor region (light blue dotted area) and the three mutation sites (marked by +) in this study. This 12 TMD topology of prestin is proposed by (Deak et al. 2005). (*modified from Dr. Kirk Beisel*).

CHAPTER 2: FROM ZEBRAFISH TO MAMMALS: EVOLUTION OF PRESTIN

I. INTRODUCTION

Prestin (SLC26A5) belongs to a distinct transporter family SLC26A consisting of 11 members as the fifth member. While all other members serve as anion transporters or channels (Dorwart et al, 2008, also refer to chapter 1), prestin is unique, functioning as a voltage-dependent motor protein responsible for the motility of mammalian OHC (Zheng et al, 2000). Mammalian prestin does not appear to transport anions across the cell membrane (Oliver et al. 2001). Although controversial studies recently suggest that prestin may also be able to transport anions such as oxalate and formate (Bai et al. 2009) as well as bicarbonate and chloride (Muallem and Ashmore 2006), this transporter activity seems to be independent from its electromotility capability (Bai et al. 2009). Prestin orthologs from NMV species such as zebrafish and chicken are electrogenic divalent/chloride anion exchangers (Schaechinger and Oliver 2007) with no motor function (Albert et al. 2007; He et al. 2003). These studies together with the fact that prestin belongs to the SLC26A family appear to suggest that prestin may have evolved from a sulfate transporter (Okoruwa et al. 2008).

During inner ear evolution, birds also have morphologically and physiologically different hair cell types which appear to be homologous with the OHC and IHC in mammals (He et al. 2003). However, to get comprehensive insight of how the function of prestin evolved, prestin orthologs from prototherian species should be studied in order to make the appropriate connections between eutherians and NMV. Moreover, monotremes such as platypus are the survivors of early branching in the mammalian evolutionary tree. The platypus (*Ornithorhynchus anatinus*, *Oanat*) cochlea is comma-shaped rather than

coiled, while the structurally and functionally different OHC and IHC are present (Fernandez and Schmidt 1963; Ladhams and Pickles 1996). Prestin orthologs from these species are evolutionary links that may offer necessary peptide sequence and structural implications of how prestin functions and evolves from the NMV transporter to the mammalian electromotility motor (Okoruwa et al. 2008).

To determine when the innovation of prestin's motor function occurred and whether it was accompanied by diminishing transport function, the motor and transport functions of the prestin orthologs from zebrafish, chicken, platypus, and gerbil (*Meriones unguiculatus*, *Mungu*) were measured in this study. Such a comparative study may reveal molecular peculiarities underlying the mechanisms of motor and/or transporter functions of prestin. It can also shed light on which amino acids are essential to the distinct function of prestin.

II. MATERIALS AND METHODS

A. Cloning of prestin orthologs

Full-length cDNAs of prestin were cloned from the inner ear of gerbil (gPres), chicken (cPres) and zebrafish (zPres). The details of cloning were described elsewhere (Albert et al. 2007; Schaechinger and Oliver 2007; Zheng et al. 2000). These plasmids (gPres: courtesy of Dr. Jing Zheng; cPres and zPres: courtesies of Dr. Dominic Oliver) were cloned into the pEGFP-N1 vector to generate EGFP fusion-proteins. The construction of platypus prestin (pPres) was done by KW Beisel, OE Okoruwa and colleagues. Correct orientation and reading frame were verified by sequence analyses.

B. Cell culture and transient transfection

Human embryonic kidney (HEK) cells were cultured in DMEM (Invitrogen, CarIsbad, CA) supplemented with 10% fetal bovine serum. For electrophysiological studies, the cells were passaged into 35-mm dishes 24 hours before transfection at a cell confluence of approximately 50-60% of the culture dish surface area. Prestin orthologs were added into the dishes using lipofectamine 2000 (Invitrogen) following the manufacturer's instructions. The amount of DNA used for each 35 mm dish was 4 μg (in 10 μl lipofectamine). For radioisotope uptake experiments, the cells were passaged into 24-well plates 24 hours before transfection, with the amount of 2 x 10^5 cells per well. The number of cells was counted using a hemacytometer (Fisher Scientific Inc., Pittsburgh, PA). The amount of DNA used for each well was 0.8 μg (in 1.6 μl lipofectamine). Fluorescence microscopy was used to determine the expression and the membrane targeting of the EGFP-prestin fusion protein during experiments for cell selection. Confocal microscopy was used for the pictures presented in this study (Matei et al. 2006).

Chinese hamster ovary (CHO) K1 cells were also used in radioisotope-labeled anion uptake experiments. This alternative cell line was used to compare the transfection rate with the HEK cells, using the same protocol and amount of DNA and lipofectamine used for HEK cells.

C. NLC measurements

NLC was measured by whole-cell voltage-clamp techniques using Axopatch 200B (Molecular Devices Corp. Sunnyvale, CA) on an upright fluorescence microscope (Leica DM LB; Leica Microsystems, Inc., NY). The cells were bathed in an extracellular medium containing (mM): 120 NaCl, 2 $MgCl_2$, 2 $CoCl_2$, 20 TEA, 10 HEPES, 10 4-AP. Recording pipettes were pulled from borosilicate glass with resistances between 2.5-4 MΩ and back-filled with solution containing (mM): 140 CsCl, 2 $MgCl_2$, 10 EGTA, 10

HEPES. Cells with obvious membrane-associated EGFP expression under fluorescence illumination were selected for NLC measurements. Membrane capacitance was measured using a two-sine-wave voltage stimulus protocol (10 mV peak at both 390.6 and 781.2 Hz) with subsequent fast Fourier transform-based admittance analysis (Santos-Sacchi et al. 2001) from a holding potential of 0 mV. The capacitive currents were sampled at 100 kHz and low-pass filtered at 5 kHz. Series resistance was compensated off-line. Data were acquired using jClamp (Scisoft, New Haven, CT) and analyzed with Igor (WaveMetrics, Portland, OR).

The NLC can be described as the first derivative of a two-state Boltzmann function relating nonlinear charge movement to voltage (Ashmore 1987; Santos-Sacchi 1991). The capacitance function is described as:

$$C_m = C_{lin} + \frac{Q_{max}\alpha}{\exp[\alpha(V_m - V_{1/2})](1+\exp[-\alpha(V_m - V_{1/2})])^2}$$

where, Q_{max} is maximum charge transfer, $V_{1/2}$ is the voltage at which the maximum charge is equally distributed across the membrane, or equivalently, the peak of the voltage-dependent capacitance, C_{lin} is linear capacitance, and $\alpha = ze/kT$ is the slope of the voltage dependence of charge transfer where k is Boltzmann's constant, T is absolute temperature, z is valence of charge movement, and e is electron charge.

The C_{lin} is proportional to the surface area of the membrane (the size of the cell). Since C_{lin} is not relevant to this study, the linear capacitance was subtracted and only the NLC was presented as a function of voltage for the data presented in the Results section. To compare the magnitude of NLC from cells with different prestin-expression level due to differences in cell size, the C_{lin} was normalized by the linear capacitance of the cells.

D. Motility measurements

To measure electromotility of transfected HEK cells, a suction pipette or microchamber was used to mechanically hold the cell and to deliver voltage commands (He et al. 1994). Microchambers were fabricated from 1.5 mm thin-wall glass tubes (World Precision Instruments, Inc., Sarasota, FL) using a Flaming/Brown Micropipette Puller (Model P-97, Sutter Instrument Company, Novato, CA) and heat-polished to an aperture diameter of ~13–15 μm. The microchamber, with a series resistance of approximately 0.3–0.4 MΩ, was mounted in an electrode holder, which was held by a Leitz 3-D micromanipulator (Leica Microsystems Inc, Bannockburn, IL). By moving the microchamber, cells in the bath could be picked up easily. The inserted cell and the microchamber formed a resistive seal (3-4 MΩ) that was mechanically stable. The electrical stimulus was a sinusoidal (100-Hz) voltage burst of 100 ms duration. Voltage commands of 400 mV (peak-to-peak) were used. Since the cells were approximately 50% inserted into the microchamber, the resultant voltage drops on the extruded segment were estimated to be 50% of the voltage applied, or 200 mV (Evans et al. 1991).

Voltage-evoked cell motion was measured and calibrated by a photodiode-based measurement system mounted on the inverted microscope (Jia and He 2005). The magnified image of the edge of the cell was projected onto a photodiode through a rectangular slit. Cell membrane motion, evoked by voltage stimuli, modulated the light influx to the photodiode. The photocurrent response was calibrated to displacement units by moving the slit a fixed distance (0.5 μm) with the image of the cell in front of the photodiode. After amplification, the photocurrent signal was low-pass filtered by an anti-aliasing filter before being digitized by a 16-bit A/D board (Digidata 1322, Molecular Devices, Union City, CA). The photodiode system had a cutoff (3 dB) frequency of 1100

Hz. The sampling frequency was 5 kHz. By averaging 200 trials and low-pass filtering at 200 Hz, cellular motion as low as 5 nm could be measured.

E. Transporter function assessment

To measure the transporter function of prestin orthologs, conventional radioisotope technique was used. [^{14}C] formate (Moravek Biochemicals, Inc., Brea, Ca) was used as the substrate and pendrin was used as the positive control according to previous studies (Bai et al. 2009). Prestin orthologs from zebrafish, chicken, platypus and gerbil were tested and the pEGFP-N1 vector was used as the negative control. The experiments were performed 24 hours after transfection in 24-well plates as described by Bai et al. (2009). Cells were first incubated in a high Cl^- solution for 30 min containing (mM): 130 NaCl, 20 HEPES, 5 KCl, 5 glucose, 2 $CaCl_2$ and 1 $MgCl_2$ (pH 7.3 and 305 Osm/L). After aspiration of this solution, the cells were incubated at room temperature for 12 min in a K gluconate solution containing 20 μM [^{14}C] formate. This K gluconate solution contains (mM): 140 K gluconate, 20 HEPES and 5 glucose (pH 7.3 and a osmolarity of 305 Osm/L). Cells were then washed three times with the cold K gluconate solution without [^{14}C] formate. After the wash, cells were lysed with 200 μl 0.5 M NaOH, and then neutralized with 0.5 M HCl. Half of the lysate was used for liquid scintillation counting to determine the [^{14}C] formate uptake and another half was used for protein analysis using Bradford assay. Triplicate wells were assayed for each plasmid with these experiments being replicated at least three times.

F. Flow Cytometry and Sterile Cell Sorting

To eliminate the influence of different transfection rate to the results of formate uptake, fluorescence flow cytometry and sterile cell sorting were performed beforehand to get 100% prestin expressing cells. Cells were detached and separated with trypsin

(Invitrogen) treatment 24 hours after transfection, and then centrifuged and resuspended in DMEM containing 10% FBS. The cell sorting was done in the Flow Cytometry Core Facility. Cytometric analysis and sorting were performed using a FACSAria (Becton-Dickinson Immunocytometry Systems, San Jose, CA) flow cytometer with an air-cooled 488 nm laser. Green fluorescence was detected with a 530/30-nm bandpass filter. Data acquisition, sorting and analysis were performed with FACSDiva software. A total of 600,000 GFP positive or negative (only for negative control) events were sorted for each sample. The collected cells were resuspended in growth medium and allowed to reattach to culture dishes for 6 hours. Dead cells were then removed by changing the medium and the surviving attached cells were washed off again and replated into a 24-well plate at a plating density of 100,000 per well. The cells were cultured for another 42 hours to insure firm attachment before the formate uptake measurements. The transporter function measurement of these cells was the same as describe above.

III. RESULTS

A. Acquisition of voltage-sensing in prestin orthologs

The NLC properties of the prestin orthologs were first measured to compare their voltage sensing capacity. HEK cells were used as a heterologous expression system to test this function. EGFP-tagged prestin orthologs from these four species were all targeted to the cell membrane 24 hours after transfection (Fig. 2-1*A*). Representative recordings of NLC measured in HEK cells transfected with zPres, cPres, pPres, and gPres are shown in Fig. 2-1*B*. gPres transfected cells exhibited a robust bell-shaped dependence on membrane potential with a peak capacitance of approximately 1.2 pF near -73 mV. Voltage-dependent NLC of gPres is characterized by the first derivative of the Boltzmann

function (heavy red lines). The means and standard deviations (SD) of the normalized NLC curve yielded values of Q_{max}/C_{lin} = 14.39 ± 3.76 fC/pF, $V_{1/2}$ = -76.49 ± 5.31 mV, and $1/\alpha = kT/ze$ = 35.2 ± 4.3 mV (n=11, Fig. 2-1*C*). The valence was calculated from α, z = 0.73 ± 0.09. These values are consistent with data reported in previous studies (Oliver et al. 2001). In contrast, when EGFP vector without prestin was expressed in the HEK cells, a flat response with no voltage dependence was observed (n=20). An example of the lack of NLC is presented in Fig. 1*B* (black lines).

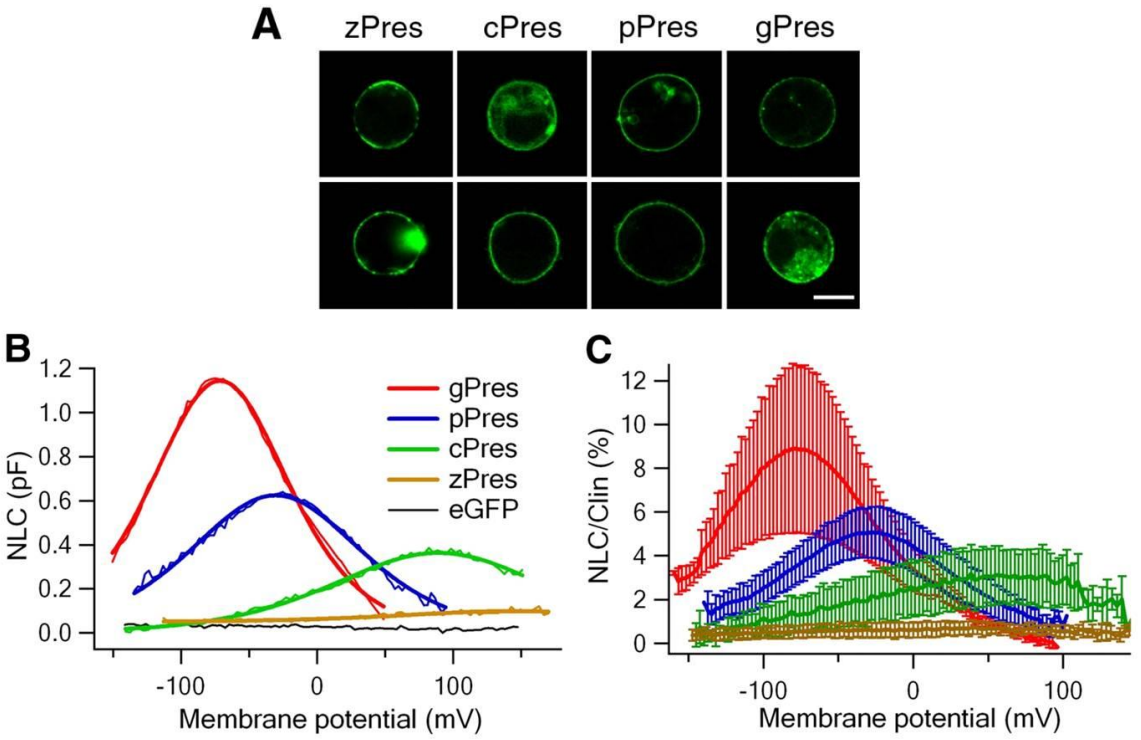

Figure 2-1. Heterogenic expression and NLC measured from prestin orthologs transfected HEK cells. ***A.*** Confocal microscopy images of HEK cells transfected with gPres, pPres, cPres, and zPres. Bar: 10 μm. ***B.*** Examples (color-coded thin lines) of NLC obtained from HEK cells transfected with gPres, pPres, cPres, and zPres. HEK cells transfected with EGFP were used as a negative control. The capacitance-voltage responses were fitted with Boltzmann function (color-coded heavy lines). Linear capacitance (C_{lin}) was subtracted from the response and only NLC was plotted. ***C.*** Pooled NLC data of the four prestin orthologs. NLC was normalized by C_{lin} and the

curves were plotted as mean ± SD (n = 11, 9, 12, 10 for gPres, pPres, cPres, and zPres, respectively).

pPres transfected HEK cells also exhibited a robust bell-shaped voltage-dependent NLC (Fig. 2-1*B*, blue lines). However, compared to that of gPres, the peak of NLC was significantly shifted to the right (depolarizing direction) with $V_{1/2}$ close to -8 mV ($P < 0.01$, compare to that of gPres). The magnitude of NLC was also significantly less than that of gPres ($P < 0.01$). Curve fitting yielded values of Q_{max}/C_{lin} = 8.4 ± 2.2 fC/pF, $V_{1/2}$ = -30.6 ± 10.7 mV, $1/\alpha$ = 39.5 ± 5.5 mV, and z = 0.65 ± 0.09, respectively (n=9, Fig 2-1C).

The NLC of cPres transfected cells exhibited a small peak that was more positively shifted than that in pPres and the magnitude of NLC was also considerably less. Fig. 2-1*C* presents the mean and SD of the normalized NLC of cPres from 11 cells. The averaged NLC response of cPres was fitted with a two-state Boltzmann function and acquired values of Q_{max}/C_{lin} = 6.3 ± 0.7 fC/pF, $V_{1/2}$ = 39.4 ± 1.8 mV, $1/\alpha$ = 55.5 ± 3.9 mV, and z = 0.46 ± 0.03, respectively.

The NLC responses from 12 zPres-expressing HEK cells were measured and an example was also shown in Fig. 2-1*B* (brown lines). The NLC had a small peak response that was more positively shifted than that exhibited by cPres transfected cells. In most cases a saturated response was not observed even at 150 mV, and could not be accurately determined due to membrane breakdown at very depolarized membrane potentials. For those cells whose a peak response could be determined within the voltage range applied, the NLC magnitude was extremely small, ~90 fF. It is noted that some uncertainty remained as to whether a two-state Boltzmann function was the most appropriate description of the voltage dependence of zPres, because only part of the voltage range

(below 150 mV) covered by NLC was accessible to capacitance measurements within a useful recording quality.

A significant shift of the $V_{1/2}$ toward negative potential was observed in cochlear OHCs when intracellular Cl^- was replaced by equal amount of I^- (Jia and He, unpublished data). Since $V_{1/2}$ of cPres and pPres was significantly shifted in the positive direction and zPres didn't show an obvious peak within the applied voltage range, It was questioned whether $V_{1/2}$ could be altered by substituting the intracellular Cl^- with equal amount of I^-. This set of experiments was important due to the uncertainty of whether the small elevation of the capacitance response was indeed voltage-dependent and whether a two-state Boltzmann function was appropriate to describe voltage-dependence of zPres. Substituting Cl^- with I^- should generate a measurable peak NLC in zPres transfected cells within the voltage range applied. More importantly, since Cl^- and I^- have different sizes, it would be interesting to see how the size and electronic structure of anion substrates influence the NLC of prestin. As shown in Fig. 2-2, the $V_{1/2}$ of gPres-, pPres-, and cPres-expressing cells all exhibited a shift as much as 100 mV to the negative direction when Cl^- was replaced by I^-. While zPres did not show an obvious saturated response in the voltage range applied with Cl^-, a peak response was detected near 50 mV when I^- was used. Parameters derived from the curve fitting with Boltzmann function yielded for zPres: Q_{max}/C_{lin} = 3.9 ± 2.3 fC/pF, $V_{1/2}$ = 8.9 ± 14.0 mV, $1/\alpha$ = 60.4 ± 19.2 mV and z = 0.48 ± 0.19, respectively. Next, Q_{max} and z value were evaluated in order to determine whether these two important parameters were different when intracellular Cl^- was replaced by I^-. The Q_{max} and z value from five gPres-transfected cells didn't show statistical difference between the Cl^-- and I^--groups. The statistical analysis of all the NLC data are listed in Table 2-1.

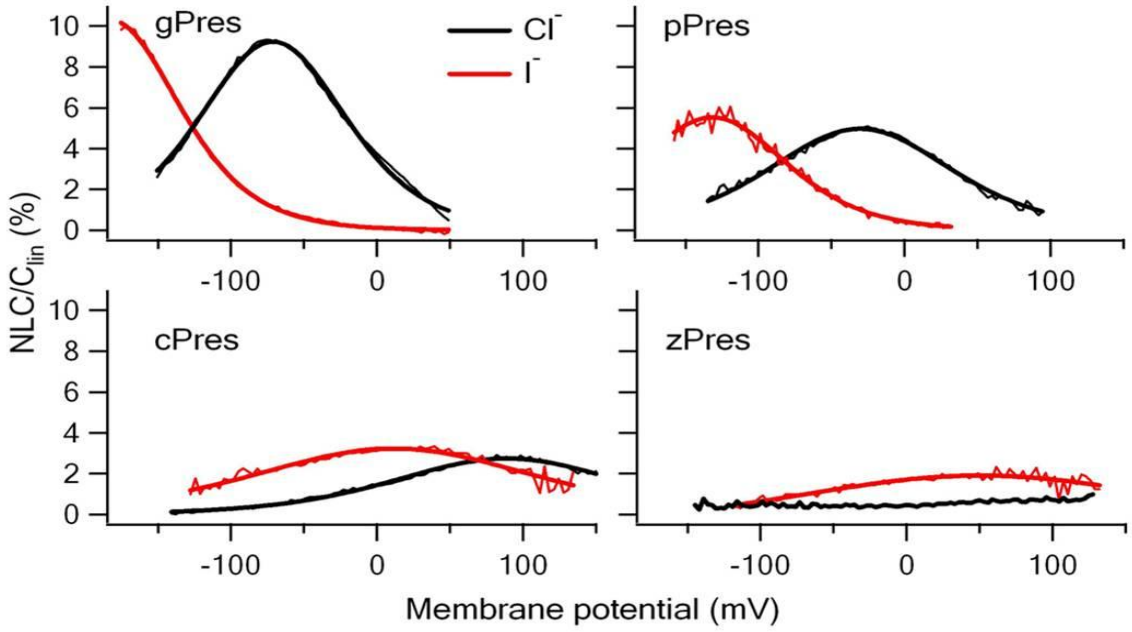

Figure 2-2. NLC changes of prestin orthologs-expressing HEK cells. NLC was measured using intracellular solutions with Cl- or I-. Thin lines represent the capacitance-voltage responses and were fitted with Boltzmann function (heavy lines).

Table 2-1: NLC parameters derived from curve fitting with Boltzmann's function

	Q_{max}/C_{lin}	$V_{1/2}$	z	$1/\alpha$
Intracellular Cl-				
gPres (n=11)	14.39 ± 3.76	-76.49 ± 5.31	0.73 ± 0.09	35.81 ± 4.07
pPres (n=9)	8.37 ± 2.22	-30.67 ± 10.61	0.65 ± 0.09	40.26 ± 5.14
cPres (n=12)	6.32 ± 0.75	39.48 ± 1.76	0.47 ± 0.03	55.35 ± 3.83
Intracellular I-				
gPres (n=5)	11.74 ± 3.19	-212.86 ± 32.82	0.80 ± 0.09	32.64 ± 4.30
zPres (n=7)	3.88 ± 2.25	8.90 ± 13.95	0.48 ± 0.19	60.37 ± 19.20

B. Attainment of motor function in prestin orthologs

The motor function is assumed to be mediated by an "actuator" in the molecule and manifested as length change in OHCs or prestin-transfected cells. The electromotility of the transfected ells was measured using a microchamber technique (Albert et al. 2007; He et al. 1994; Zheng et al. 2000). Since a spherical cell cannot effectively change its surface area, the cells were drawn into the suction pipette (microchamber), which produced a dumbbell shape (Fig. 2-3*A*). Sinusoidal voltage bursts were delivered to the cells via the microchamber with an estimated voltage of 200 mV (peak-to-peak). This voltage stimulation was large enough to generate saturated response, as the examples shown in Fig. 2-3*B*. The gPres-expressing cells exhibited robust motility on the extruded segment, with the magnitude of 85 ± 27 nm (n=8, the red line). The motile response evoked in pPres-expressing cells was also obvious though smaller, with the magnitude of 53 ± 14 nm (n=6, the blue line).

Twenty-three zPres-expressing cells, all exhibiting clear membrane labeling, were probed for electromotility using sinusoidal voltage bursts of 300 mV (peak to peak) for the extruded segment. Given a resting membrane potential of approximately -5 mV for HEK cells, a sinusoidal stimulus of 300 mV would result in membrane voltage swings from -165 mV to +155 mV. Such large potential changes should be sufficient to evoke motility (if any) even though the $V_{1/2}$ of the zPres-mediated NLC was shifted towards more positive potentials. Signs of electromotility, however, were not detected in any of the zPres-expressing cells. An example of the lack of motility is presented in Fig. 2-3*B* (the brown line). Motility of cPres-positive cells was also measured using the same voltage protocol for zPres. None of the 20 cells measured showed any time-registered response to the sinusoidal voltage stimulus (Fig. 2-3*B*, the green line).

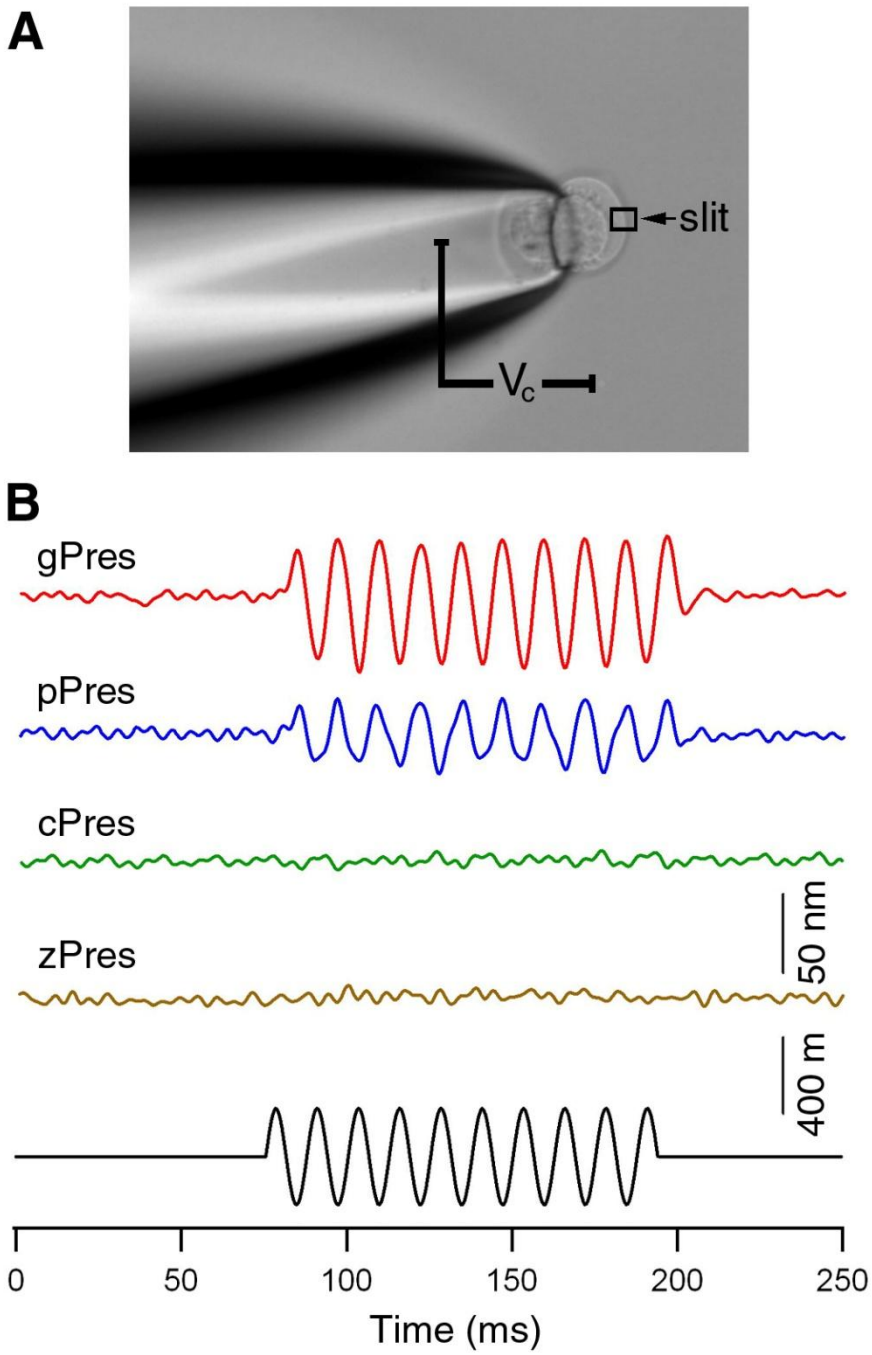

Figure 2-3. Somatic motility measured from HEK cells transfected with gPres, pPres, cPres, and zPres, respectively. ***A.*** Diagram showing motility measurement using the microchamber technique. The cell was approximately 50% inserted into the microchamber and length change of the extruded segment was measured. ***B.*** Examples of motile responses of the cells transfected by gPres, pPres, cPres, and zPres, respectively. The electrical stimulus was a 100-Hz sinusoidal voltage burst with duration of 100 ms.

C. Characterization of transport function

A recent study showed that prestin transfected CHO cells show the capability of exchanging extracellular [^{14}C] formate with intracellular chloride (Bai et al. 2009). A similar technique was applied to compare the transporter function of the prestin orthologs from the four species. Both the HEK and CHO cell lines were used in this study. The human pendrin (SLC26A4) was used as a positive control for it is a verified anion transport (Dossena et al. 2009). The basal formate uptake in negative control groups was about 60 pmol of formate per ~200,000 cells in both the EGFP-transfected cells (60 ± 6 pmol) and the untransfected cells [64 ± 5] (Fig. 2-4A). Cells transfected with human pendrin showed a robust transport capability with the value of 225 ± 15 pmol. Both zPres (92 ± 7 pmol) and cPres (70 ± 5 pmol) increased significantly comparing to that of the EGFP control (one-way ANOVA, $P < 0.01$ and $P < 0.05$, respectively). By contrast, the formate uptake was not changed in cells transfected with pPres (67 ± 6 pmol) or gPres (64 ± 6 pmol). To rule out that this trend of transport activity was due to the differences of transfection efficiency, flow cytometry experiments were performed to examine the transfection rate of prestin orthologs. The results are presented in Fig. 2-4B. Regression analysis showed that transfection rates among the 4 different prestin orthologs had no significant effect on formate uptake ($P = 0.92$). To rule out the possibility of variation in formate uptake being attributed to cell loss during the assay procedure, the total protein concentration in each well was determined (Fig. 2-4C). The limited formate uptake by cells expressing mammalian prestin was certainly not due to cell loss during preparation, for the amount of protein was similar for all groups in all the experiments.

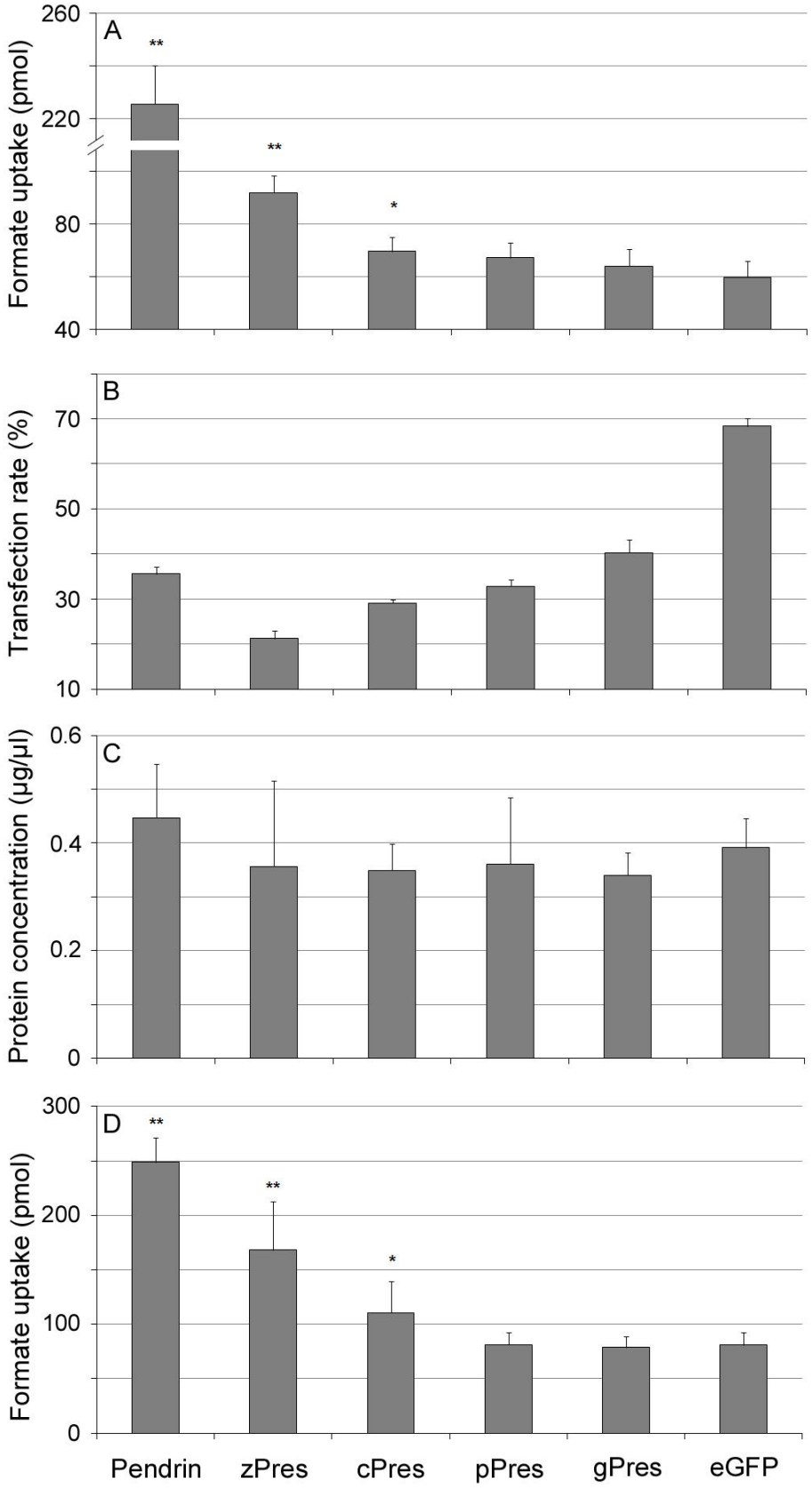
A
Formate uptake (pmol)
260
220
80
40
**
**
*
B
Transfection rate (%)
70
50
30
10
C
Protein concentration (µg/µl)
0.6
0.4
0.2
0
D
Formate uptake (pmol)
300
200
100
0
**
**
*
Pendrin
zPres
cPres
pPres
gPres
eGFP

Figure 2-4. Transport activity of prestin orthologs. ***A.*** ^{14}C-labeled formate uptake of HEK cells transfected by human pendrin, zPres, cPres, pPres, gPres, and EGFP only, respectively. The experiments were performed on 24-well plates 24 hours after transfection, with the original inoculation of 200,000 cells per well. The value was the averaged formate uptake per well. All the data were acquired from 3 wells in each plate and repeated 3 times. ** $P < 0.01$. * $P < 0.05$, compare to that of EGFP. ***B.*** Flow cytometry data showing the transfection rate of the 7 plasmids. The transfection rate was determined by the percentage of cells expressing fluorescence through flow cytometry calculation. ***C.*** Protein analysis using Bradford Assay. Protein concentrations of HEK cells in each well of a 24-well plate transfected with different prestin orthologs vary from 0.34 to 0.44 μg / μl. No statistical significance among different groups was found ($P = 0.07$, one-way ANOVA, single factor). ***D.*** Formate uptake after cell sorting. The cells re-inoculated in each well were 100,000 after cell sorting and formate uptake was performed 48 hours afterwards. ** $P < 0.01$. * $P < 0.05$, compare to that of EGFP.

The transfection rates among four different species varied between 20 and 40 percent of the total cells in each well (Fig. 2-4B). gPres and pPres had higher transfection rates than zPres and cPres. A higher transfection rate would mean that more prestin expressing cells could contribute to formate transport and this might have an influence to the results. To overcome this bias, fluorescence-activated flow cytometry was used to isolate EGFP-positive (transfected) cells. Formate uptakes were then measured from only EGFP-positive cells. Before uptakes were measured, the total number of the cells in each well was counted to ensure that the number of cells was the same among different groups. Both zPres (168 ± 44 pmol) and cPres (111 ± 29) showed a higher increase in formate uptake over the base line (81 ± 12 pmol in EGFP transfected cells) with statistical significance (Fig. 2-4D. one-way ANOVA, $P < 0.01$ in both cases). The transporter

function of pPres (81 ± 11 pmol) and gPres (79 ± 10 pmol) were again not statistically significant compared with that of the control. The transport capability of prestin orthologs of NMV demonstrated in this study was consistent with a previous study using an electrophysiological approach (Schaechinger and Oliver 2007).

To further confirm if the formate uptake activity of prestin orthologs is similar to that of other SLC26A family members, a well-characterized blocker of anion transporter, 4,4'-diisothiocyanatostilbene-2,2'-disulfonic acid (DIDS) (Bai et al. 2009), was added to the K^+-gluconate solution together [^{14}C] formate. HEK cells transfected with four constructs including pendrin, zPres, gPres and EGFP were tested and the results are presented in Fig. 2-5*A*. The uptakes of [^{14}C] formate in cells expressing all four constructs was significantly inhibited in the presence of 0.5 and 1 mM DIDS. In pendrin-transfected cells, the inhibition was dose-dependent. Transport in all other constructs, including zPres, were maximally inhibited (13-15 pmol) in the presence of 0.5 mM DIDS (Fig. 2-5*A*). Similar results were also observed in sorted cells, as shown in Fig. 2-5*B*. The transporter function decreased significantly in pendrin transfected cells (112 ± 5 pmol), and to about 25 pmol in all prestin orthologs in the presence of 1 mM DIDS.

A previous study used CHO cells to examine the anion transporter function of prestin (Bai et al. 2009). In that study Bai et al. (2009) was able to demonstrate significant anion uptake for both formate and oxalate. Based on these data, CHO cells were also used to determine the transport function of prestin orthologs. Our results showed that CHO cells had a much lower transfection rate than that of HEK cells (data not shown). The highest transfection rate observed in CHO cells was less than 10% for both pendrin and zPres. This contrasted to approximately 35% and 20%, respectively, in HEK cells. The higher transfection rate in HEK cells would be advantageous for detecting low levels of

transport activity, since more prestin-expressing cells would contribute to the formate uptake. As expected, prestin orthologs-transfected CHO cells showed less formate uptake (15-25 pmol / 200,000 cells) under the same conditions for the HEK cells. Despite this, zPres and cPres exhibited significant uptake of formate compared with the control groups. As seen with the HEK cells, formate uptake by pPres- and gPres-expressing cells was not different from the EGFP controls.

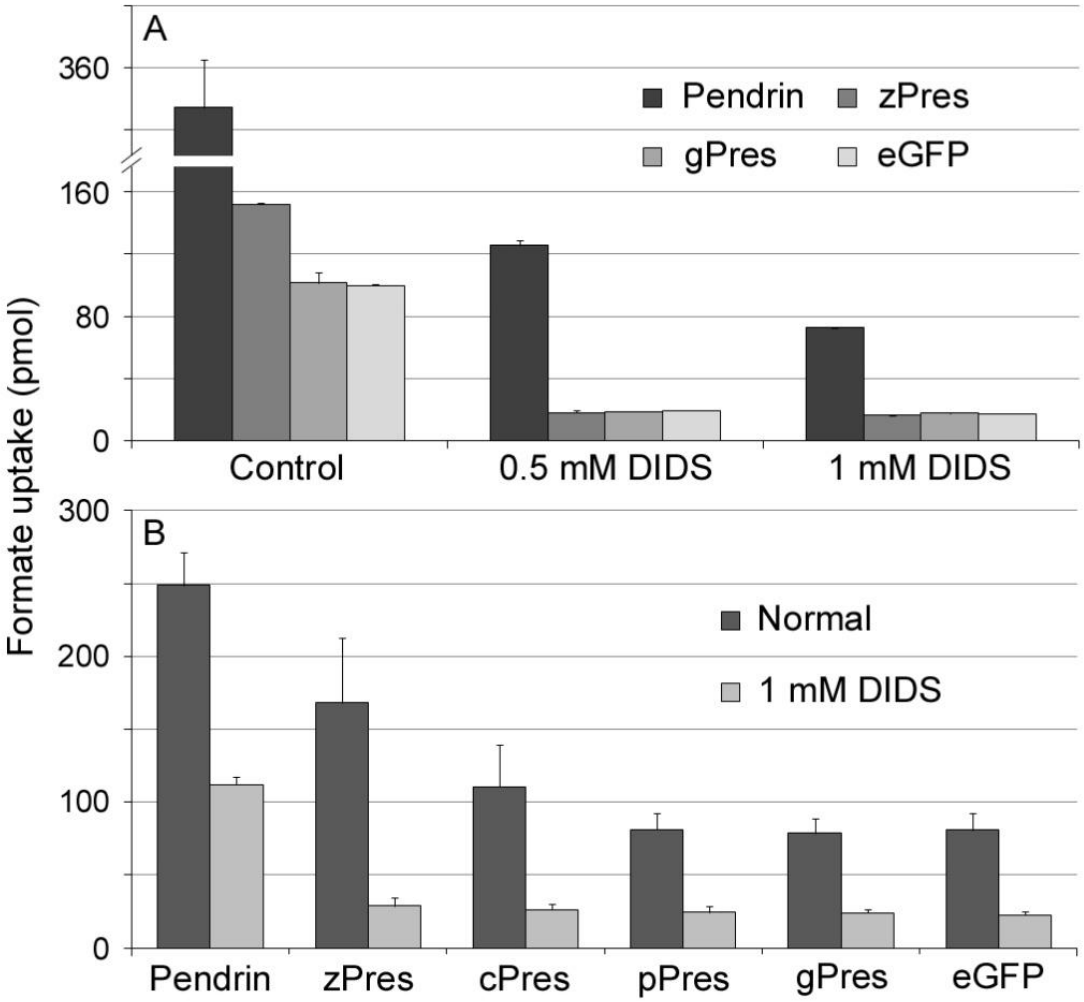

Figure 2-5. Inhibition of transport function by an anion transporter blocker, DIDS. ***A.*** Inhibition of formate uptake by DIDS. The incubation time with [^{14}C] formate was 12 minutes. ***B.*** Inhibition of formate uptake by DIDS after cell sorting. The incubation time with [^{14}C] formate was 10 minutes.

IV. DISCUSSION

Mammalian prestin is unique among the SLC26A gene family members in its capability of functioning as a motor protein. The characteristics of prestin orthologs for anion transport, NLC and cell membrane movement were evaluated. zPres and cPres were used as representatives of the NMV orthologs. Platypus is a prototherian species that displays features shared with both reptiles and mammals (Okoruwa et al. 2008). By measuring motor and transport functions, it was shown for the first time the reciprocal relationship between anion transport properties and NLC (Fig. 2-6). Inverse graded changes were observed in the four species such that as transporter function diminishes from zPres to gPres, the NLC characteristic shifted from positive to negative voltages and the amplitude of NLC became more prominent (Fig. 1-1). This was accompanied by the acquisition of somatic motility in both pPres and gPres (Fig. 1-3). It appears that the motor function of prestin is, as previously thought (Franchini and Elgoyhen 2006; Rajagopalan et al. 2006; Weber et al. 2003; Zheng et al. 2002), a newly derived molecular property exclusive to the therian lineage. Acquisition of electromotility appears to be at the expense of anion transport.

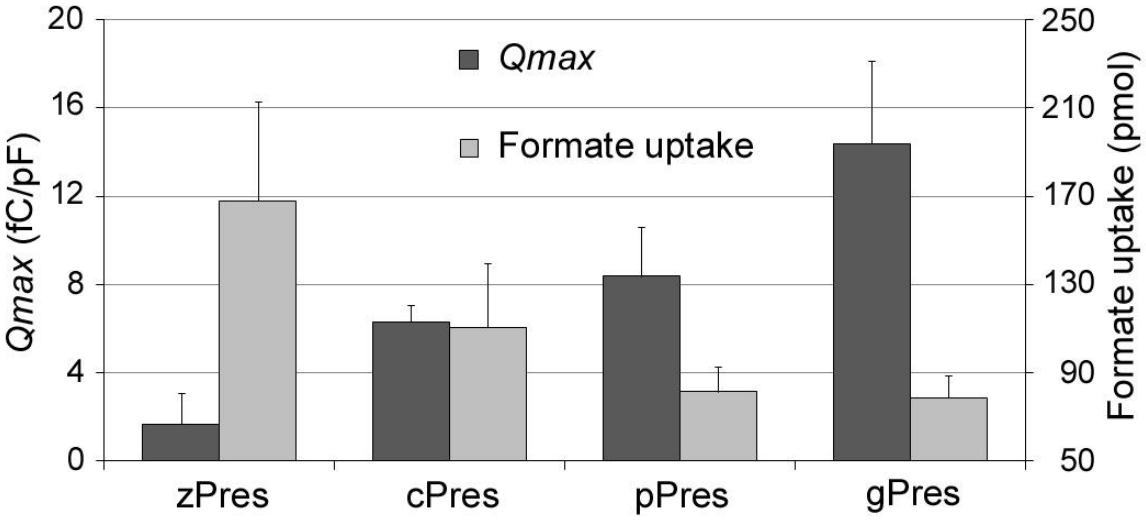

Figure 2-6. Comparison of the Q_{max} (left axis) and formate uptake (right axis) of prestin orthologs. The Q_{max} was used as the representative of NLC. Notice the reciprocal evolutionary relationship of NLC and the transporter function.

Interestingly enough, this evolutionary trend of motility function has its structural clue indicated in the previous study (Okoruwa et al. 2008). Highly conserved sequences in membrane spanning regions of mammalian prestin were identified and thought to contain sequences critical for the motor function (Chapter 1, III B). These conserved sites also exist in prototherians. The NLC and motility measured in pPres transfected cells (Figs 2-1 and 2-3) clearly support the supposition that motility first appear in the prototherian species (Franchini and Elgoyhen 2006). There is an amino acid of homology of 89% within the meEM domain between the eutherian consensus sequence and that of platypus (Okoruwa et al. 2008); unpublished data). It is still unknown which changes in these conserved regions have led to the acquisition of the motor function. Nevertheless, the fact that NLC of pPres is significantly smaller and right shifted compared to those of gPres suggests that a gradual change may have occurred as the therian lineage evolved. cPres, with a 58% amino acid identity to rat prestin (Schaechinger and Oliver 2007), exhibits a small NLC. Whereas zPres, with ~50% amino acid identity to mammalian prestin (Albert et al. 2007), does not have any similarity in these regions compared to its mammalian orthologs.

NLC is thought to be generated by charge movements, similar to the gating current seen in voltage-dependent ion channels. The study by Oliver et al. (2001) suggests that the intracellular anions such as Cl^- and HCO_3^- function as the voltage sensor in prestin (Oliver et al. 2001). According to this model, anions binding to sites with high affinity

are translocated across the membrane by the transmembrane voltage: toward the extracellular surface upon hyperpolarization and toward the cytoplasmic side in response to depolarization. The translocation triggers conformational changes in the protein that subsequently change its surface area in the plane of the plasma membrane. The presence of NLC in zPres and cPres and their responses to intracellular substitution of Cl^- by I^- may suggest a common mechanism of charge movement seen in the mammalian prestin. However, lack of motor function in zPres and cPres indicates that the charge movements and motor function may evolve independently, although the two are believed to be fully coupled in mammalian prestin (Ashmore 1989; Santos-Sacchi 1989; Wang et al. 2010). It should be pointed out that the possibility of small motility (less than 5 nm) in zPres and cPres could not be rule out, which might be missed due to the resolution limit of the measurement system used in this study.

Through replacement of intracellular Cl^- with I^-, discernable NLC peak of zPres was able to identified. Replacement of intracellular Cl^- with I^- resulted in a significant shift of $V_{1/2}$ in all 4 species (Table 2-1). The mechanism of this shift is unknown. However, it has been reported that the anion affinity of prestin is $I^- \approx Br^- > NO3^- > Cl^- > HCO3^- > F^-$ (Oliver et al. 2001). This order is similar to the anion-binding to pendrin and some chloride channels (Fahlke et al. 1997; Scott and Karniski 2000). It is possible that the size of anion may play an important role as the bulk of I^- is significantly larger than Cl^-. Another important factor might be the size of the hypothetical tunnel that allows anions to bind to a specific site and translocate across the membrane.

Although prestin and prestin orthologs from mammals and NMV all exhibit NLC, it is controversial whether mammalian prestin can transport anions. While some studies show that only prestin orthologs from the NMV are divalent/chloride anion exchangers

(Albert et al. 2007; Schaechinger and Oliver 2007), others have demonstrated that mammalian prestin also exhibits this function (Bai et al. 2009; Muallem and Ashmore 2006). The data from this study indicate that there are quantitative differences in the transport capabilities of the four prestin orthologs compared (Fig. 2-4). zPres showed a formate uptake capability that was substantially higher than that in the EGFP control or other prestin orthologs. cPres showed a small but statistically significant greater level of formate transport than the control. These results were substantially verified by the results after cell sorting (Fig. 2-4D). The transporter function of the two mammalian orthologs, however, was not statistically different from the control groups. It should be pointed out that the lack of transporter function of mammalian prestin is not due to the difference in transfection rate among the prestin orthologs (Fig. 2-4B). In fact, mammalian prestins had higher transfection rates than those of NMV orthologs. It was further demonstrated that formate transport by zPres and cPres was less robust compared with the pendrin paralog. Therefore, the NMV orthologs of SLC26A5 appear to be the least effective anion transporters when compared to other SLC26A paralogs.

Transport capability was measured from both HEK and CHO cells using the same standard technique used in virtually all previous studies. By further measuring formate uptakes from only transfected cells after cell sorting, the influence of transfection rate on measurements could be minimized. In previous studies, formate uptake was measured from the total population that contained both transfected and non-transfected cells. If the transfection rate is low, only a small proportion of cells that are transfected can contribute to specific transport activity. Therefore, the specific transport activity of interest can potentially be masked by the background uptake. Our approach using cell sorting should significantly improve sensitivity to detect weaker transportation of substrates across the

cell membrane since the measurements were only taken from the transfected, EGFP-positive cells. Even with the improved approach, we did not observe transport capability greater than the background uptake in pPres and gPres. Although we cannot completely rule out the possibility that mammalian prestin still retain some extremely weak transport capability, it strongly suggests that such transport capability diminishes during functional evolution of prestin.

In conclusion, there appears to be an inverse relationship between motor and anion transport functions during functional evolution of prestin. Motor function appears to have only emerged in mammalian prestin and the gain of motor function is concurrent with diminished transport capabilities. However, the fact that non-mammalian prestin orthologs can transport anions suggests that prestin is evolved from an anion transporter.

CHAPTER 3: IDENTIFICATION OF THE MOTOR AREA OF PRESTIN

I. INTRODUCTION

The voltage sensor and the actuator are the two putative fundamental structural features of prestin underlying its unique voltage-dependent motile function. However, little is known about the amino acid sequences or regions associated with these two functions (Dallos and Fakler 2002; Oliver et al. 2001). The studies in Chapter 2 as well as some previous studies (Albert et al. 2007) have demonstrated that NMV prestin orthologs also have small charge movement following the membrane potential. In contrast, the motility of prestin is newly evolved functions, which only exists in mammals (Albert et al. 2007; He et al. 2003) (also refer to Chapter 1). In order to be the motion generator, the mobile region is predicted to be clustered and large enough to account for significant changes of the molecular shape (Rybalchenko and Santos-Sacchi 2008).

A number of attempts to identify critical regions in the prestin sequence were recently achieved. Most provide only indirect evidence relating the structure to the function of prestin (Bai et al. 2009; Deak et al. 2005; He et al. 2006; Kumano et al. 2009; Navaratnam et al. 2005; Oliver et al. 2001; Pasqualetto et al.; Zheng et al. 2005). Mutations causing alterations in prestin membrane expression and the NLC properties are commonly observed (Navaratnam et al. 2005; Zheng et al. 2005). Failure of membrane targeting disables function measurements of these mutations. Altered NLC properties have only indirect implications on prestin's motility function. Only the mutation V499G/ Y501H, with a marginal or no NLC signature, was shown to eliminate the motor function

of prestin and subsequently lead to the loss of hearing in mutant mice, while the mechanism or related structural changes remain unknown (Dallos et al. 2008). Another study identified another potential chloride binding site on which the mutation also abolished NLC, while the motility measurement was not done (Bai et al. 2009). Further investigation is needed and more precise areas should be defined and studied to determine the candidate motor of the prestin molecule. A combination of bioinformatic methods and mutagenesis studies seems to be promising based on recent progress.

Evolutionary studies combined with comparative genomic and bioinformatic analyses have identified highly conserved sequences which are well conserved among mammalian species but highly variable among prestin paralogs and NMV orthologs (Okoruwa et al. 2008). Most of these sites or regions are located in the membrane-spanning sequence from residues 66 to 503 (Chapter 1, III B) and are thought to be essential for the newly evolved motor function of prestin. Substituting the C-terminus or N-terminus (Navaratnam et al. 2005; Zheng et al. 2005) of prestin with the analogous C or N-terminus portion of Pendrin (SLC26A4) or PAT1/CFEX (SLC26A6), two closely related SLC26A proteins, have been done previously. These chimeric mutants are unable to be delivered to the plasma membrane (Zheng et al. 2005) or result in loss of electrophysiological function (Navaratnam et al. 2005). However, chimeric proteins constructed from prestin orthologs which are closer in evolution and less different in sequence to each other may avoid such pitfalls. In this study, I first attempted to swap the central core containing the essential motor region between NMV and mammalian prestin orthologs to determine whether this region is important for prestin's unique motility function.

One motif in this large 438-residue conserved membrane spanning region, residing in the external loop 2 (EL2) of the 12-TMD model, contains a segment of 11 amino acids and appears to be a newly derived feature for mammalian prestin (Okoruwa et al. 2008). This segment was named as the minimum essential motif for electromotility motor (meEM), and was hypothesized to confer the motor function to prestin. To test this hypothesis, chimeric proteins were constructed by swapping corresponding residues from zPres (158-171, MVNGTNSSLVVNI), and cPres (158-176, ISVGYNSTNATDASDY YSL) with those from gPres (158-168, IPGGVNATNGT). The NLC and somatic motility were measured in transfected HEK cells. A gain of function in chimeric prestins of both zPres and cPres with both NLC and motility was observed while the transporter function still maintained.

II. MATERIALS AND METHODS

A. Swapping of N-, C- termini of prestin orthologs

Amino acids 66 to 503 of gPres are defined as the central hydrophobic core (Sulfate transporter core, SulpTP core) based on the 12-TMD model (Oliver et al, 2001). The equivalent regions in cPres and zPres sequences were identified by amino acid sequence alignment using BLAST. They are amino acids 67 to 509 for both cPres and zPres.

Chimeric mutants swapping the N-, C- termini and the central hydrophobic core of prestin were constructed by restriction enzyme digestion and re-ligation of orthologs from gerbil, chick and zebrafish (kindly provided by JL Pecka and KW Beisel, Fig. 3-1). Two restriction enzyme sequences, Sspl and DraIII, were incorporated in advance into these SulpTP core N- and C- junctions without altering the amino acid sequences. The introduction of these two sites was done by site-directed mutagenesis in the pEGFP-N1

expression clones using the QuikChange XL site-directed mutagenesis kit (Stratagene, La Jolla, CA). The following descriptors for the N- or C- terminal chimeras were CGG (N-terminus from cPres with gPres contributing the central SulpTP core and C- terminus, similar hereafter), ZGG, GCC, GZZ, GGC, GGZ, CCG and ZZG for the initial single domain swapping chimeras. Construction of the central hydrophobic core chimeras obtained the homomeric N- and C-termini CGC, ZGZ, GCG and GZG chimeric clones. These initial constructs were produced in the pCR-II vector (Invitrogen, Carlsbad, CA) utilizing the multiclone sites and the orientation of the reading frames were inserted in the reverse orientation from the lacZ reporter. Once constructed, these sequences were excised and inserted into pEGFP-N1 expression vector in correct orientation to generate the C- terminal EGFP fusion proteins. All constructs were verified by nucleotide sequence analyses of the entire constructed sequences.

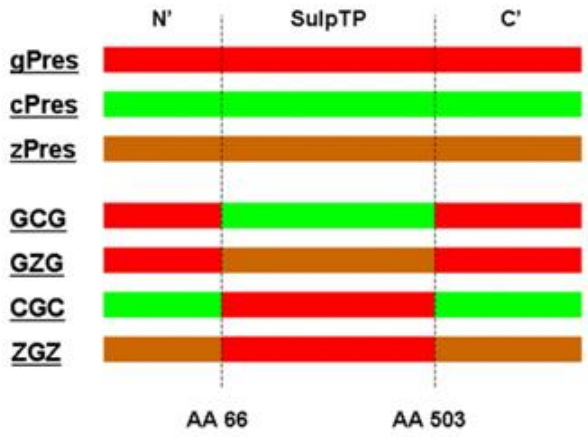

Figure 3-1. Schematic diagram showing the construction of chimeras swapping the N-, C- termini and SulpTP cores of gPres, cPres and zPres. Three portions of the whole peptide, the N-, C-termini and sulphate transporter core (SulpTP, from amino acid 66 to 503), are separated by dashed lines. Chimeric proteins were constructed by swapping the three portions of gPres, cPres and zPres. GCG means the chimeric protein with N-, C- termini from gPres and SulpTP Core from cPres. A total of 12 chimeric proteins were constructed.

B. Swapping of the putative motor region

Prestin orthologs gPres, cPres and zPres were used for the swapping construction (Fig. 3-2). Amino acids 158 to 168 of gPres were defined as the meEM motif (Okoruwa et al, 2008) and the equivalent regions in cPres and zPres sequences were identified by amino acid sequence alignment using BLAST. The residues from gPres meEM motif (IPGGVNATNGT) were exchanges with those from zPres (158-171, MVNGTNSSLVVNI) or cPres (158-176, ISVGYNSTNATDASDYYSL) by restriction enzyme digestion and re-ligation. These initial constructs were produced in the pCR-II vector (Invitrogen, Carlsbad, CA) utilizing the multiclone sites. Once constructed, these sequences were excised and inserted into pEGFP-N1 expression vector to generate EGFP fusion proteins. Clones were kindly provided by JL Pecka and KW Beisel. Chimeric proteins zPres or cPres with gPres meEM motif were designated as Zf(g) or Ck(g), respectively. Correct orientation and reading frame of all the constructs were confirmed by sequence analyses.

Figure 3-2. Schematic diagram showing the construction of chimeric SLC26A5 swapping the putative motor region (the meEM motif). gPres sequence is shown in blue and zPres is shown in red. Chimeras swapping the meEM motif are Gb(z) and Zf(g), respectively. The primary sequences for the swapped regions are also indicated. Equivalent chimeric proteins swapping sites of gerbil and chicken SLC26A5 were also constructed (not shown on the diagram).

C. Cell Culture and Transient Transfection

Human embryonic kidney (HEK) cells were used as the heterogeneous expression system for all the constructs. The culturing and transient transfection protocols were the same as those described in Chapter 2. Briefly, cells were cultured in DMEM solution, supplemented with 10% fetal bovine serum and passaged into 35 mm dishes 24 hours before transfection. Prestin or mutants (4μg) were introduced into the cells using 10μl lipofectamine (Invitrogen) following the protocol from the manufacturer.

D. Confocal Imaging

Membrane-associated expression of prestin mutations was again verified 24 hours after transfection by confocal imaging, performed on a LSM 510 microscope (Zeiss, Thornwood, New York) using a 40X water immersion objective.

E. NLC Measurements

NLC measurements using whole cell patch clamp techniques were performed 24-48 hours after transfection on cells with membrane-associated EGFP expression. Details were described in Chapter 2. Briefly, cells were detached by trypsin treatment 24 hours after transfection and bathed in extracellular solution with ion channel blockers. Recording pipettes were filled with solution also containing ion channel blockers. Membrane capacitance was measured using a two-sine-wave voltage stimulus protocol (SantosSacchi, 1991) and amplified by Axopatch 200B (Axon Instruments). JClamp (SciSoft Company) was used for data acquisition and analysis. NLC were fitted with a two-state Boltzmann function (Ashmore, 1989; Santos-Sacchi, 1991) and the derivative parameters were statistically analyzed.

F. Motility Measurements

Somatic motility of the transfected HEK cells were measured and calibrated by a photodiode-based system (He et al., 1994; Zheng et al., 2000, also refer to Chapter 2).

The electrical stimulus was a sinusoidal voltage burst of 100 ms duration with the voltage of 400 mV. With an average of 200 trials and low-pass filtering set at 200 Hz, cellular motion as low as 5 nm could be detected and should follow the waveform of the stimulus.

G. Transporter Function Assessment

A conventional radioisotope technique was used to measure the transporter function and [^{14}C] formate (Moravek Biochemicals, Inc., Brea, Ca) was applied as the substrate. Human pendrin and pEGFP-N1 vector were used as the positive and negative control, respectively, according to previous studies (Bai et al., 2009) and studies in Chapter 2. Formate uptake capability of HEK cells transfected with of gPres, cPres, zPres, Zf(g) and Ck(g) was tested 24 hours after transfection. The details of the experiments are provided in Chapter 2. The incubation time of the cells with [^{14}C] formate was 10 min.

III. RESULTS

A. Prestin ortholog domain Swapping

The membrane spanning region (SulpTP core) of prestin is highly conserved in mammals and the majority of amino acid substitutions are predominately confined to the cytoplasmic N- and C- termini (Okoruwa et al., 2008). The integrity of SulpTP core thus may be essential for the function of prestin and the substitution of N-, C- termini may help to elucidate this question. To test the functional properties of the evolving meEM, chimeric proteins were constructed swapping the N- and C- termini and the SulpTP of gPres and cPres / zPres. The heterogenic expression, membrane-targeting and NLC of these chimeric proteins were examined and compared in the transfected HEK cells. Theoretically, if the highly conserved SulpTP core of mammalian prestin contains elements which is essential for the motility function, chimeric proteins with gPres SulpTP

(e.g., gPres SulpTP with zPres N-, C- termini, ZGZ) should demonstrate NLC on transfected cells, while those without the mammalian meEM motif should have no NLC (e.g., zPres SulpTP with gPres N-, C- termini, GZG).

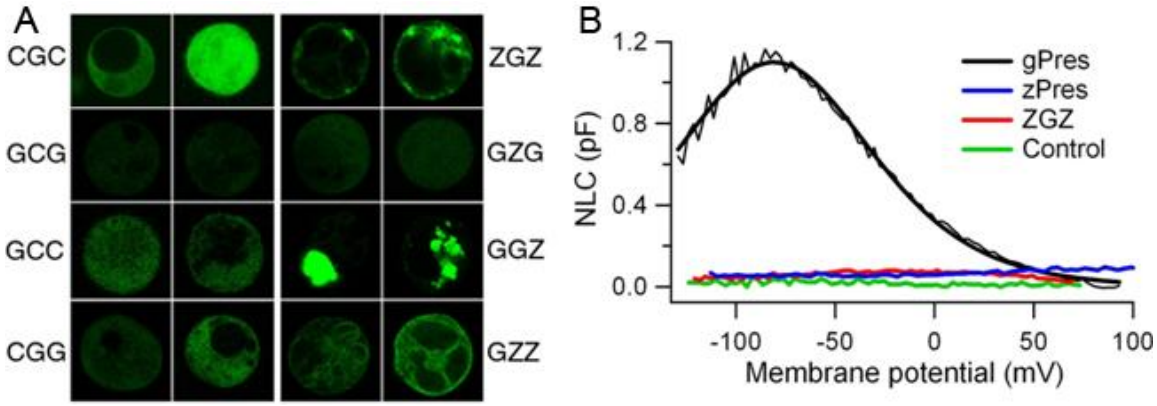

Figure 3-3. Expression pattern and NLC of the domain-swapping chimeras. ***A.*** Confocal images of HEK cells transfected by chimeric DNA. Different chimeras showed various expression patterns. Chimera ZGZ exhibited weak membrane-associated fluorescence as well as dense expression in some restricted areas in cytoplasm. GGZ showed dense and punctuate expression in perinuclear region of the cell. Expressions in most other constructs were distributed throughout the cytoplasm, at various fluorescence intensity and/or granular size (e.g., CGC, GCG, GZG, GCC, CGG and GZZ). ***B.*** NLC of zPres, gPres and chimera ZGZ transfected HEK cells. Cells with no EGFP expression were used as negative control. Chimera ZGZ, containing the mammalian SulpTP, showed only minimum NLC, compared to the robust NLC of mammalian prestin. Other chimeras with no membrane bound expressions exhibited no apparent NLC (data not shown).

Totally twelve chimeras were constructed (Fig. 3-1). These included constructs with homogenic (e.g., CGC and CGC) or heterogenic (e.g., GCC and CGG) N- and C- termini. Confocal images showed that each chimera had different expression pattern, varying in both the expression level and cytoplasmic localization (Fig. 3-3*A*). To characterize these patterns, two cells for each chimera were selected to represent the expression pattern of

that construct. Most constructs were expressed in cytoplasm without obvious membrane targeting (e.g., CGC, GCG, GCC, CGG, GZG and GZZ). Some others only expressed in restricted areas in the perinuclear region of the cell (e.g., GGZ). Among the twelve constructs, only one (i.e., ZGZ) had fluorescence expression on the cell membrane. Whole-cell patch-clamp recordings showed that ZGZ transfected HEK cells didn't display voltage-dependent NLC (Fig. 3-3*B*, red lines) compared to zPres and the negative control. Others without surface expression also didn't show any voltage-dependent NLC (data not shown).

B. Gain of NLC in Zf(g) and Ck(g)

Next, the functional properties of swapping constructs in a more restricted area, the Zf(g) and Ck(g) were examined. Chimeric prestin clones constructed exhibited cell surface expression 24 hours after transfection, as evident by the membrane-associated EGFP expression (Fig. 3-4*A*). The function of the voltage sensor was measured, manifested as NLC (Ashmore 1989; Santos-Sacchi 1991). gPres-transfected cells showed a bell-shaped NLC with a peak capacitance of approximately 1.2 pF near -73 mV (Fig. 3-4B). Voltage-dependent NLC data of gPres were fitted with the first derivative of the Boltzmann function (Santos-Sacchi 1991). In contrast, zPres only exhibited weak voltage-dependent NLC as demonstrated before (Albert et al. 2007; Tan et al. 2010a) (also in Chapter 2). The NLC of zPres had a small elevated peak response significantly shifted in the positive voltage direction (Fig. 3-4*B*). The saturated response in most cases was not clearly seen even at 150 mV and could not be determined due to membrane breakdown at very large depolarized membrane potentials. However, when zPres chimeric protein with gPres residues 158-168 was measured, a significant gain of magnitude of NLC with left shift of $V_{1/2}$ was observed. NLC responses from 8 Zf(g)-

expressing cells were measured. Curve fitting using Boltzmann function yielded values of mean and standard deviation of Q_{max}/C_{lin} = 4.7 ± 1.2 fC/pF, $V_{1/2}$ = 7.3 ± 14.4 mV, and $1/\alpha = kT/ze$ = 54 ± 12.3 mV (Fig. 3-4*B*). cPres chimera with the same gPres site, the Ck(g), was also constructed. Ck(g) was also expressed on the membrane (Fig. 3-5*A*). Although cPres has small NLC with no motility (Tan et al., 2010), substitution of cPres residues 158-176 with those from gPres residues 158-168 also conferred Ck(g) with large NLC (Fig 3-5*B*).

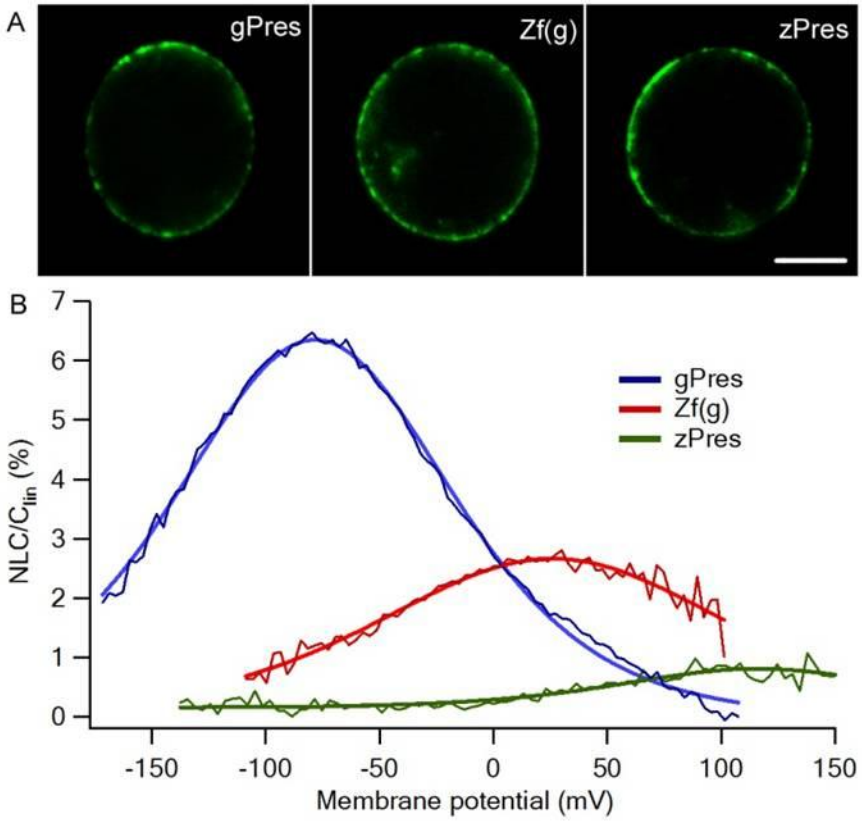

Figure 3-4. Heterogenic expression and NLC of gPres-, Zf(g)- and zPres-transfected HEK cells. ***A.*** Representative confocal microscopy images of cells transfected with gPres, Zf(g) and zPres. The white bar represents 10 μm. ***B.*** Examples of NLC from gPres-, Zf(g)- and zPres-transfected HEK cells. The capacitance-voltage responses were fitted with the Boltzmann function (lighter-colored thicker lines). NLC is normalized by linear capacitance (C_{lin}).

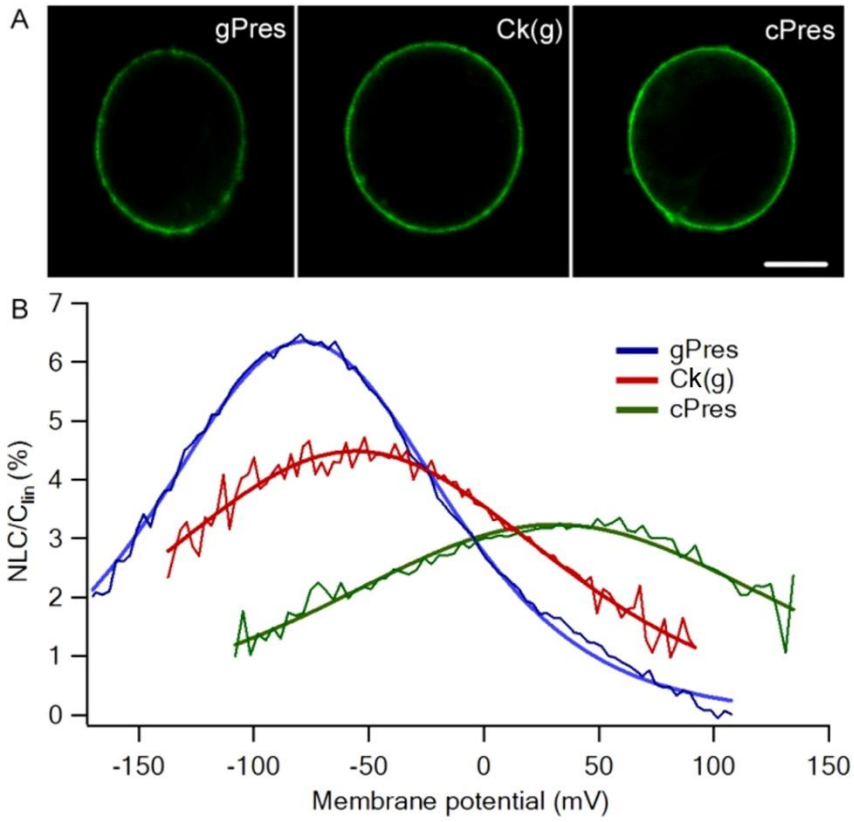

Figure 3-5. Heterogenic expression and NLC of gPres-, Ck(g)- and cPres-transfected HEK cells. ***A.*** Confocal images of transfected cells (bar: 10 μm). ***B.*** Examples of NLC from gPres-, Ck(g)-, and cPres-transfected HEK cells (color coded). Light color-coded thick lines represent fitting curves with the Boltzmann function.

C. Gain of Motor function in Zf(g) and Ck(g)

The motor function of prestin is presumably mediated by the "actuator" in the molecule and manifested as length change. Electromotility of Zf(g)-transfected HEK cells was measured using the microchamber technique (He et al. 1994). GPres-transfected HEK cells showed robust motility and were used as a positive control. As shown in Fig. 3-6*A*, Zf(g)-transfected HEK cells also exhibited motility when the cells were stimulated with 100 Hz sinusoidal voltage burst. The amplitude was 33 ± 9 (mean ± SD, n=8). In contrast, none of the thirty two zPres-transfected cells measured exhibited

any somatic motility. Somatic motility from Ck(g) was also measured and its motility was also observed. An example of the motile response of Ck(g) is presented in Fig 3-6*B*.

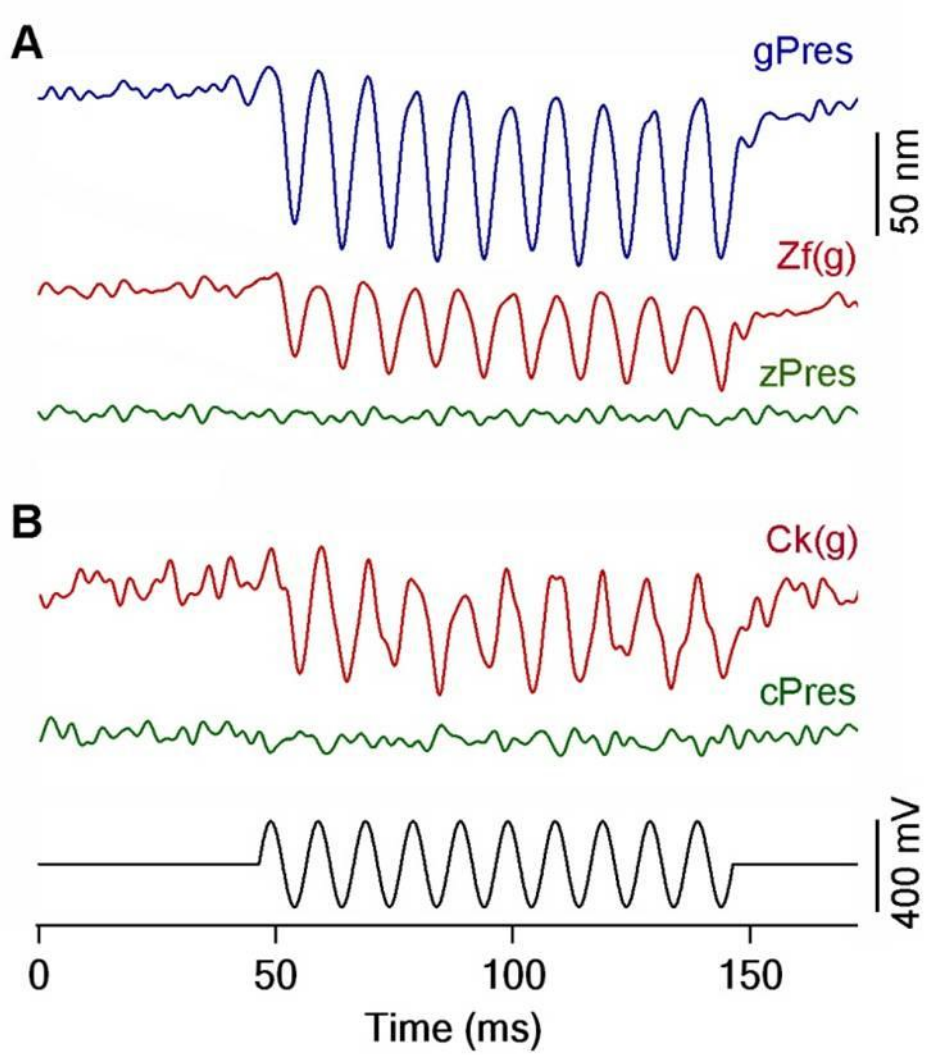

Figure 3-6. Motility of gPres-, Zf(g)-, zPres-, Ck(g)- and cPres-transfected HEK cells. (A) Somatic motility (color-coded) of gPres-, Zf(g)- and zPres-transfected HEK cells. (B) Somatic motility of cPres- and Ck(g)-transfected HEK cells. The electrical stimulus was a 100-Hz sinusoidal voltage burst with duration of 100 ms.

D. Transport Function of Chimeric Prestin is Retained

Since prestin orthologs from zebrafish and chicken demonstrate the ability to

transport anions (Schaechinger and Oliver 2007; Tan et al. 2010b), it is questioned whether the gain of motor function of Zf(g) and Ck(g) occurs at the expense of a loss of the transport function. The anion transport function was measured using standard radioactive-labeled formate ion uptake assays (Bai et al. 2009; Tan et al. 2010b). The human SLC26A4 paralog, pendrin, was used as positive control (Dossena et al. 2009). The vector expressing the EGFP was used as the negative control. HEK Cells transfected with human pendrin fusion protein showed a robust transport capability (140 ± 17 pmol /200,000 cells, the same below) comparing to that of the EGFP (47 ± 3 pmol) (Fig 3-7). Since zPres and cPres also demonstrate transport capabilities (Tan et al. 2010b), zPres and cPres were also included for comparison. As shown, cells transfected with zPres showed a higher transport capability (72 ± 8 pmol). Interestingly, Zf(g) transfected HEK cells also exhibited an increased transport activity (69 ± 6 pmol) similar to that of the zPres. The transport functions of cPres (50 ± 3 pmol) and Ck(g) (50 ± 2 pmol) are also the same as each other. These results suggest that anion transporter activity of the chimeras is retained.

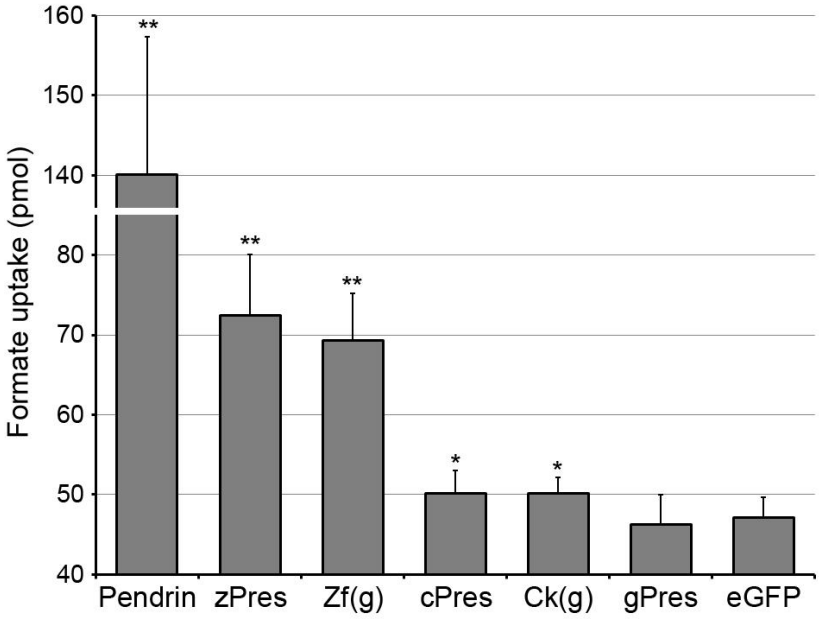

Figure 3-7. Formate uptake of zPres-, Zf(g)-, cPres, Ck(g) and gPres-transfected HEK cells. Human pendrin was used as the positive control and EGFP-only vector was used as negative control. All the data were acquired from 3 wells in each plate and repeated 3 times. (one-way ANOVA: ** $P < 0.01$; * $P < 0.05$, compare to EGFP).

IV. DISSCUSSION

A. Functional co-evolution of N-, C- termini and central core

The hydrophobic core of mammalian prestin (amino acids 66 to 503) is highly conserved and the majority of amino acid substitutions are predominately confined to the cytoplasmic N- and C- termini (Okoruwa et al. 2008). Chimeras swapping the C-terminus of prestin with those of other paralogs were studied previously, encountering a variety of expression problems, most of which were not properly transported to the cell membrane (Zheng et al. 2005). Furthermore, previous studies of series truncations on N-, C- termini also assumed that the entire or certain areas of N-, C- termini were important for specific molecular processes such as proper protein folding, assembly into cytoplasmic vesicles, transportation to the membrane and homo-oligomerization (Navaratnam et al. 2005; Zheng et al. 2005). Chimera proteins constructed from prestin orthologs which were evolutionarily more close to each other might avoid such pitfalls, and thus might be good models to test the functional properties of the evolving meEM motif. Instead, our study indicated that these chimeric proteins encountered similar expressional variations and membrane targeting difficulties. In addition to that, ZGZ, the only one that did have membrane-associated expression failed to show expected NLC. Similar membrane targeting problems have been reported in other swapping studies (Navaratnam et al. 2005; Zheng et al. 2005). These results suggested that instead of an

impact on a specific process, there appears to be a more general functional co-evolution of N- terminus, central hydrophobic core and C- terminus, with the N- and C- termini exhibiting the great sequence plasticity.

B. Gain of motor function with the putative motor region

The results of this study show for the first time that substitution of an eleven amino acids region conferred motor function to the electrogenic anion transporters zPres and cPres. On the basis of this experimental data, it was propose that this peptide segment represents the therian motor region of prestin. The fact that the gain of motor function is not accompanied by a loss of transport function suggests that separate domains are responsible for the motor and transport properties of prestin. This is consistent with the conclusion of a previous study (Bai et al. 2009).

A comparison of the members of the vertebrate *SLC26A5* gene family show many similar features in both the genomic exon organization and deduced protein sequences. The newly acquired physiological feature of the voltage-dependent prestin movement is predicted to reflect a region within the SulpTP core domain that has a high degree of insertion and deletion occurrence when compared with the eutherian and the NMV prestin peptide sequences. Furthermore, the lack of conservation among the NMVs should indicate that a stretch of insertions and deletions and non-conserved amino acid substitutions could provide a platform for the acquisition of motor-like properties in SLC26A5. Previous analyses identified a strong candidate stretch of amino acids within the EL2 of the SulpTP core domain [according to the 12 TMD model of (Deak et al. 2005)] that fits these criteria [i.e., the meEM motif, (Okoruwa et al. 2008)]. This site is represented by the gPres residues 158-168 (IPGGVNATNGT). The database of eutherian SLC26A5 protein sequences has increased with over 30 eutherian species with

the recent inclusion of prestin sequences from echolocating bat and whale species (Li et al. 2008; Li et al. 2010). This emEM motif is extremely conserved with no polymorphisms observed, even in the prestin proteins of the echolocating species. In contrast, this region is variable among the NMV orthologs and exhibits the greatest region of insertion and deletion occurrence within the SulpTP core (Okoruwa et al., 2008). Sequence comparisons between the eutherian and the NMV orthologs have shown that the size of this region is longer in NMV orthologs, lacks a prolyl residue, and usually has only one glycyl residue.

C. Mechanism underlying the gain of motor function of the chimeras

Two current topological models of mammalian prestin feature a SulpTP core domain of either 10 or 12 transmembrane spanning regions (Dallos and Fakler 2002; Deak et al. 2005; Navaratnam et al. 2005; Oliver et al. 2001). Based on these models, the meEM motif in the EL2 segment is either in an intracellular or extracellular loop, respectively. This is the first time that it has been shown that substituting a non-TMD plays a critical role for the gain of function. Comparison of EL2 regions of zPres, cPres and gPres reveals that the 158-168 segment in gPres is shorter and contains a prolyl and three glycyl residues. The rigidity at the prolyl residue is speculated to provide the mechanical tension necessary to translate internal charge movement into expansion and contraction of the molecule which promotes somatic motility on a microsecond time scale. Further studies are needed before this possibility can be confirmed.

CHAPTER 4: MECHANISMS UNDERLYING VOLTAGE SENSING OF PRESTIN

I. INTRODUCTION

Intracellular Cl^- ions are thought to work as extrinsic voltage sensor (Dallos and Fakler 2002; Oliver et al. 2001) or allosteric modification of prestin (Bai et al. 2009; Rybalchenko and Santos-Sacchi 2008). In either model, Cl^- ions are assumed to bind to specific sites in the prestin molecule. Positively charged amino acids in the pore or transport anion tunnel region are believed to play an important role in voltage sensing, possibly by serving as anion binding sites during this process.

Based on sequence analysis between prestin and its paralogs or NMV orthologs, mutations of conserved or unconserved positive amino acids in the putative TMDs of prestin have been studied intensely (Bai et al. 2009; Deak et al. 2005; He et al. 2006; Kumano et al. 2009; Navaratnam et al. 2005; Oliver et al. 2001; Pasqualetto et al.; Zheng et al. 2005). However, how prestin senses voltage is still unclear. It is hypothesized that the size or the charge location of the side chain of amino acids is an important factor for prestin function. To test this hypothesis, three positively charged amino acids (R197, K227 and K449) in the predicted α-helical TMD were selected for study based on sequence alignment of prestin paralogs and orthologs. Series substitutions using mutually positive amino acids (R to K and K to R) were constructed and studied, assuming that R and K are only different in size and charge orientation of the side chain. Negative (R / K to E) or neutral (R / K to A) mutations were also constructed and studied.

II. MATERIALS AND METHODS

A. Alignment of prestin paralogs and orthologs

SLC26A5 paralog and ortholog multiple alignments were done using Clc protein work-bench (Okoruwa et al. 2008), showing in Fig. 4-1. Six paralogs (SLC26A3-7 and A9), all of which are verified functional transporters, were selected for the comparison (Fig. 4-1*A*, *C* and *D*). Fifteen mammalian orthologs were used for the ortholog alignment (Fig. 4-1*B*). Positively charged amino acids in the putative membrane spanning regions according to both the ten (Deak et al. 2005; Oliver et al. 2001) and twelve (Rajagopalan et al. 2006) TMD models were considered. Three evolutionarily unique amino acids were selected. R197 is highly variable in prestin paralogs and NMV orthologs, while highly conserved in mammalian prestin orthologs (Fig. 4-1, *A* and *B*). K227 and K449 are the only positively charged amino acids which are conserved in all the prestin paralogs and orthologs (table 4-1; Fig. 4-1, *C* and *D*). The goal of these comparisons is to identify specific sites which may account for the unique voltage-dependency of prestin, or serve as the ubiquitous anion binding sites for the SLC26A transporter family.

B. Site specific mutagenesis

Full-length cDNAs of prestin were cloned from the inner ear of gerbil, and the details of cloning were described elsewhere (Albert et al. 2007; Schaechinger and Oliver 2007; Zheng et al. 2000). The gPres plasmid (courtesy of Dr. Dominic Oliver) was cloned into the pEGFP-N1 vectors to generate GFP fusion-proteins. Single site mutations at the three sites of interest were constructed by overlapping PCR using site mutagenesis kit from Invitrogen. All clones were kindly provided by JL Pecka and KW Beisel. The original arginine (Arg or R) or Lysine (Lys or K) at these three sites were mutated to R or K, glutamate (Glu or E) or alanine (Ala or A), respectively. Double (any two of the three

sites were mutated) and triple (all the three sites were mutated) mutations were also constructed, using the same site mutagenesis kit, restriction enzyme digestion and re-ligation. Correct orientation and reading frame were verified by sequence analyses.

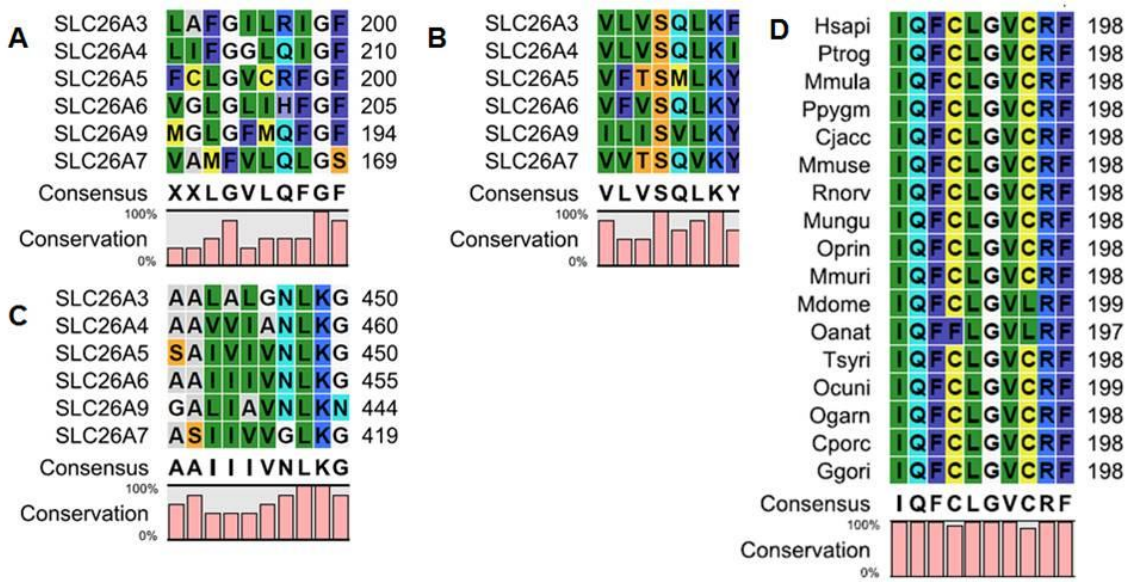

Figure 4-1. Alignment of SLC26A5 paralogs and orthologs showing the conservation of the three selected positive amino acids. ***A.*** Alignment of prestin paralogs (SLC26A3-7 and A9) from human showing that R197 is non-conserved in prestin paralogs. ***B*** and ***C.*** Alignment of prestin paralogs from human showing that K227 and K449 are both highly conserved in all the prestin paralogs. ***D.*** Alignment of SLC26A5 orthologs from 15 mammalian species showing that R197 is highly conserved in all the 15 mammalian orthologs. The animal species listed in the alignment are (from top to bottom): human, chimpanzee, macaque, orangutan, marmoset, mouse, rat, gerbil, opossum, rabbit, bushbaby, guinea pig and gorilla, respectively.

C. Cell culture and transient transfection

Human embryonic kidney (HEK) cells were used as the heterogeneous expression system for all the constructions. Cell culture and transient transfection protocols were described in Chapters 2 and 3. Briefly, cells were cultured in DMEM, supplemented with

10% fetal bovine serum and passaged into 35 mm dishes 24 hours before transfection. Prestin or mutants (4μg) were introduced into the cells using 10μl lipofectamine (Invitrogen) following the protocol from the manufacturer.

Table 4-1: Conserved amino acids within the transmembrane regions of the mammalian SLC26A paralogs

		Residue group	Hydrophobic	Polar	Charged
Transmembrane region location	1	93-109		G100	D96
	2	114-134	A115 L117 L126 P132	G125 Y127	
	3	144-161	F150	G148 S154	
	4	199-224	L204 L224	Q209 G218	
	5	231-250	A236	T234 S243	K246
	6	276-394			
	7	305-328	P310		
	8	356-377	A366 V368		
	9	394-414	A396 F407	G398 N401	
	10	431-451	A432	G448	
	11	458-474	V458 L459 L467	Q473	K468
	12	499-519		G506	

The highly conserved amino acids within equivalent regions of SLC26A5's twelve transmembrane regions are provided. Two of the three positively charged residues are highly conserved and denoted K246 and K468, which are equivalent to the SLC26A5 residues K227 and K449, respectively.

D. Confocal Imaging

Membrane-associated expression of prestin mutants was verified by confocal imaging. The membrane of transfected cells was labeled by di-8-ANEPPS (25 μM, 10 min in room temperature) 24 hours after transfection. Confocal imaging was performed on LSM 510 microscope (Zeiss, Thornwood, New York) using a 40X water immersion objective. The EGFP and di-8 fluorescence were both excited with a 488 nm Argon laser but detected separately in different channels ranging from 500-530 nm (green) and 650-710 nm (red), respectively. Co-localization of fluorescent signals indicates the membrane associate expression of the fusion protein.

E. NLC Measurements

NLC measurements using whole cell patch clamp techniques were performed 24-48 hours after transfection on cells with membrane-associated EGFP expression. Details were described in Chapter 2. Briefly, cells were detached by trypsin treatment 24 hours after transfection and bathed in extracellular solution containing blockers of ion channels. Recording pipettes were filled with solution containing the blockers of ion channels. Membrane capacitance was measured using a two-sine-wave voltage stimulus protocol (Santos-Sacchi 1991) and amplified by Axopatch 200B (Axon Instruments). JClamp (SciSoft Company) was used for data acquisition and analysis. NLC was fitted with a two-state Boltzmann function (Ashmore 1989; Santos-Sacchi 1991) and the derivative parameters were statistically analyzed.

III. RESULTS

A. Mutations containing site R197 showed difficulties on membrane expression.

A total of twenty one mutants on the three selected sites were constructed. They are the mutually positive substitutions swapping Arg and Lys, neutral substitutions using Ala and negative substitutions using Glu. Confocal microscopy showed differences in the expression patterns of the mutant peptides (Fig. 4-2). All the positive mutations as well as some of the negative and neutral ones, including K449A, K227E and K449E, showed robust green fluorescence expression on the membrane, similar as that of the wild type gPres (Fig. 4-2, the upper left panel). Some others showed relatively high expression level but were distributed mostly in the cytoplasm, including K227A, R197E+K227E and the triple E mutations (Fig. 4-2, the lower left panel). K227A+K449A had a lower expression level but mostly on the membrane (Fig. 4-2, the upper right panel). All other neutral or negative mutations containing site R197 showed a cytoplasmic fluorescence without obvious membrane expression, including R197A, R197A+K227A, R197A+K449A, triple A, R197E, R197E+ K449E (Fig. 4-2, the lower right panel). The lack of membrane-targeting of these mutations was further indicated by the absence of measurable NLC (no NLC in six to eight cells recorded, data not shown). The membrane expression of the constructs is summarized in Table 4-2. Six out of eight neutral and negative mutations containing site R197 exhibited an absence of membrane localization. Although the single negative mutant R197E was not expressed on the membrane, the double negative mutant R197E+K227E and triple E rescued membrane expression.

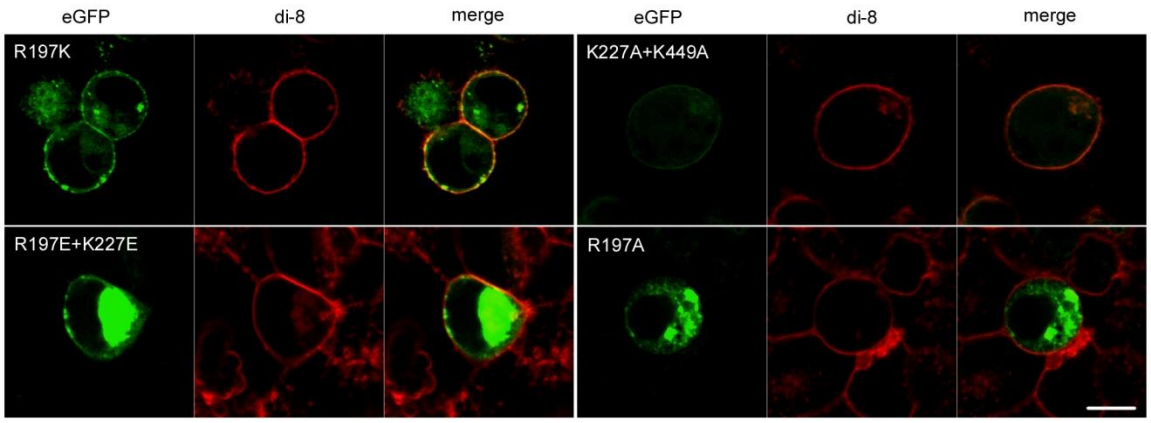

Figure 4-2. Confocal images of transfected HEK cells showing different expressing patterns of the mutants. The upper left panel: example of cell with good expression level and membrane-binding; The lower left panel: good expression level with low membrane-association; The upper right panel: low expression level while mostly on the membrane; The lower right panel: good expression level with no membrane-targeting. Cell membrane was labeled by di-8-ANEPPS and the co-localization of EGFP (left column) and di-8 (middle column) was indicated by orange in the merged images (right column). Bar: 10 μm.

Table 4-2: Membrane-Associated Expression of the Mutants.

Site of the mutations	R vs K	R &K to A	R & K to E
197	+	-	-
227	+	w	+
449	+	+	+
197 + 227	+	-	W
197 +449	+	-	-
227 + 449	+	+	+
Triple	+	-	W

+ means relatively high expression, w means low expression and - means no expression on the membrane, respectively.

B. Mutations on sites R197, K227 and K449 showed significant influences on NLC

The voltage sensor of prestin is manifested as the characteristic NLC (Ashmore 1989; Santos-Sacchi 1991), or voltage-dependent charge movement that arises from the redistribution of charged "voltage sensors" across the membrane. NLC is characterized by a bell-shaped dependence on membrane potential which is well fitted by the first derivative of Boltzmann's function (Ashmore 1989; Santos-Sacchi 1991). Statistical results of the curve-fitting with Boltzmann's function are listed in table 4-3. Compared to that of the wild type gPres, the amplitudes of Q_{max} decreased significantly in all the mutants except K227E. Alterations in $V_{1/2}$ were also obvious in most constructs, shifting to either negative or positive voltage. Changes on slope factor α were also observed. K227E+K449E, one of the double negative mutations, had an outlier Q_{max} with the value ranging from 2 to 50. The negative mutation triple E had no measurable NLC in all the seven cells recorded.

a. Mutual positive substitution had significant influence on prestin function

The study of mutual positive mutations (R to K and K to R) was based on the assumption that they different only in size or charge location of the side chain, instead of the charge itself (Fig. 4-3, the insert). Fig. 4-3 shows the representative capacitance – voltage curve of single, double and triple mutual positive mutations. gPres showed a robust bell-shaped dependence on membrane potential with a peak capacitance of approximately 1.2 pF near -73 mV (the black line). R197K also had a typical NLC with a decreased peak capacitance (0.6 pF) and right-shifted peak voltage (-58 mV) (the red lines). On the other hand, the NLC of R197K + K227R showed a further decreased peak capacitance (0.4 pF) while accompanied by a left-shifted peak voltage (-92 mV, the blue

lines). More interestingly, the voltage operation range (defined as the voltage range within which the probability for prestin to switch from the expanded to the contracted state varies between 10% and 90%. See Rybalchenko and Santos-Sacchi, 2008) was also decreased, which is represented by the increase of α. This decrease in voltage operation range was also observed in another positive constructs, R197K+K449R, which also contains mutation at site R197. The NLC of the triple R/K mutant decreased even more, with a minimum peak capacitance of 0.25 pF and a peak around -40 mV (the green lines).

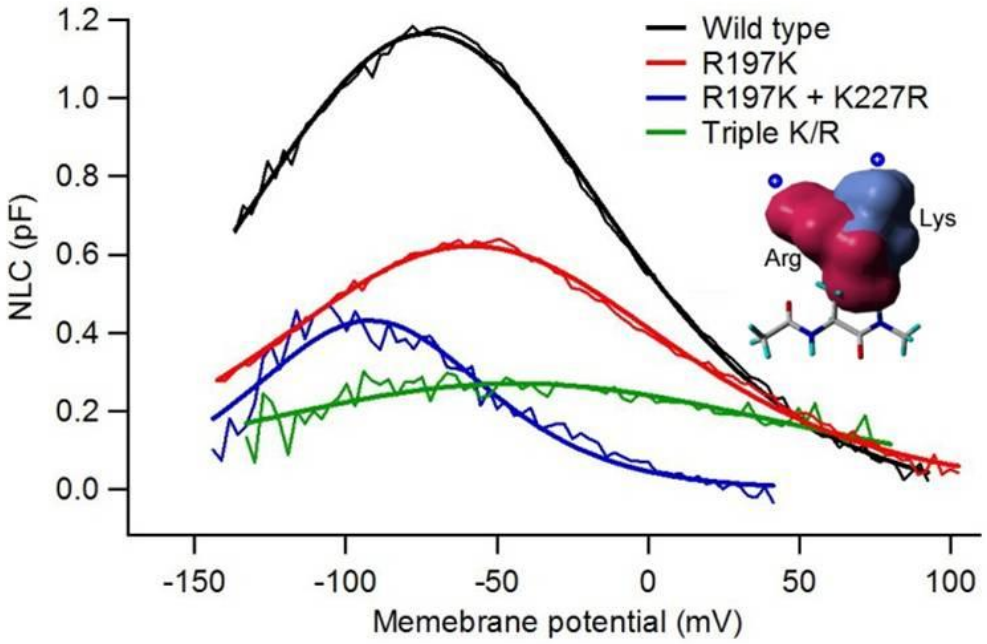

Figure 4-3. NLC obtained from HEK cells transfected with mutual positive mutations. Representative capacitance-voltage curves of R197K, R197K + K227R and the triple K/R are shown. Wild type gPres is a positive control. The original NLC curves are shown in color-coded thin lines and fitted with Boltzmann function shown in heavy lines. Linear capacitance (C_{lin}) was subtracted from the response and only NLC plotted. The insert is the Van der Waals' topography showing differences on the size and the charge location of the side chain between Arg (showing in red) and Lys (showing in blue).

Table 4-3. NLC parameters of the mutants derived by curve fittings (mean ± SD)

Constructs	Q_{max}/C_{lin} (fC/pF)	$V_{1/2}$ (mV)	α (1/V)	Number of cells
WT prestin	14.39 ± 3.76	-76.49 ± 5.31	28.42 ± 3.50	11
R197K	7.25 ± 2.55**	-52.10 ± 9.82**	22.14 ± 5.13	8
K227K	6.37 ± 2.37**	-40.24 ± 5.92**	21.63 ± 4.03	8
K449K	8.62 ± 2.69**	-60.18 ± 6.68**	22.46 ± 4.31	8
R197K+K227R	2.03 ± 0.67**	-92.10 ± 7.70**	40.37 ± 8.32**	8
R197K+K449R	4.40 ± 1.64**	-116.00 ± 14.36**	35.42 ± 3.11*	8
K227R+K449R	8.67 ± 1.86**	-51.75 ± 10.21**	25.43 ± 1.27	6
Triple K/R	8.21 ± 1.30**	-56.94 ± 15.72	16.34 ± 2.44**	8
R197A	-	-	-	8
K227A	6.75 ± 3.63**	-125.98 ± 31.88**	30.43 ± 2.86	7
K449A	5.70 ± 1.22**	-38.01 ± 11.52**	20.36 ± 5.68	8
R197A+K227A	-	-	-	6
R197A+K449A	-	-	-	6
K227A+K449A	2.67 ± 1.60**	-113.74 ± 23.03**	35.08 ± 2.86*	8
Triple A	-	-	-	6
R197E	-	-	-	8
K227E	13.10 ± 0.54	-117.67 ± 13.32**	27.05 ± 1.93	6
K449E	4.21 ± 1.65**	-49.29 ± 23.94	29.31 ± 2.62	6
R197E+K227E	5.54 ± 2.33**	-33.55 ± 12.42**	18.50 ± 1.95**	6
R197E+K449E	-	-	-	8
K227E+K449E	-	-32.58 ± 17.51**	13.16 ± 7.50**	6
Triple E	-	-	-	7

* $p < 0.05$; ** $p < 0.01$ compared with that of the wild type.

b. Replacement with Ala or Glu also showed cumulative effect on NLC other than the expression pattern

When replaced by the neutral amino acid Ala, with only a methyl group on the side chain, the positive charges were neutralized and the size of the side chain was shortened. While substituted by the negative amino acid Glu, the positive charges were changed into negative ones. It was reasoned that these substitutions might give more clues as to how the size and/or character of charges of the R group can alter the voltage sensing of prestin. While nearly half of these mutants had the problem of membrane expression or lost the NLC, the voltage-dependent NLC of the remaining constructs may be informative. As shown in Fig. 4-4, the single neutral mutation K449A (Fig. 4-4A, the red lines) had a decreased peak capacitance (0.5 pF) and the double one K227A + K449A (Fig. 4-4A, the blue lines) had an even smaller peak capacitance (0.4 pF). Same cumulative effects were also observed in negative mutants, K227E (Fig. 4B, the red lines) had a peak capacitance close to that of the wild type (0.8 pF), while that of R197E + K227E (Fig. 4-4B, the blue lines) decreased to 0.2 pF. In triple E, the voltage-dependent capacitance change is diminished to near zero (Fig. 4-4B, the green lines).

C. Pooled data showing the relationships between $V_{1/2}$/Q_{max} and α

As indicated by their definitions, parameters derived by curve fitting with Boltzmann's function may have implications on prestin functional features. To speculate the mechanism underlying the alterations of voltage sensing in these mutations, the relationships between NLC parameters were further investigated by correlation analysis using the pooled data. Q_{max}, $V_{1/2}$ and α were all changed to various degrees in these mutations. Taken together, a negative relationship between $V_{1/2}$ and α (Fig. 4-5A) while no positive relationship between Q_{max} and α (Fig. 4-5B) were observed.

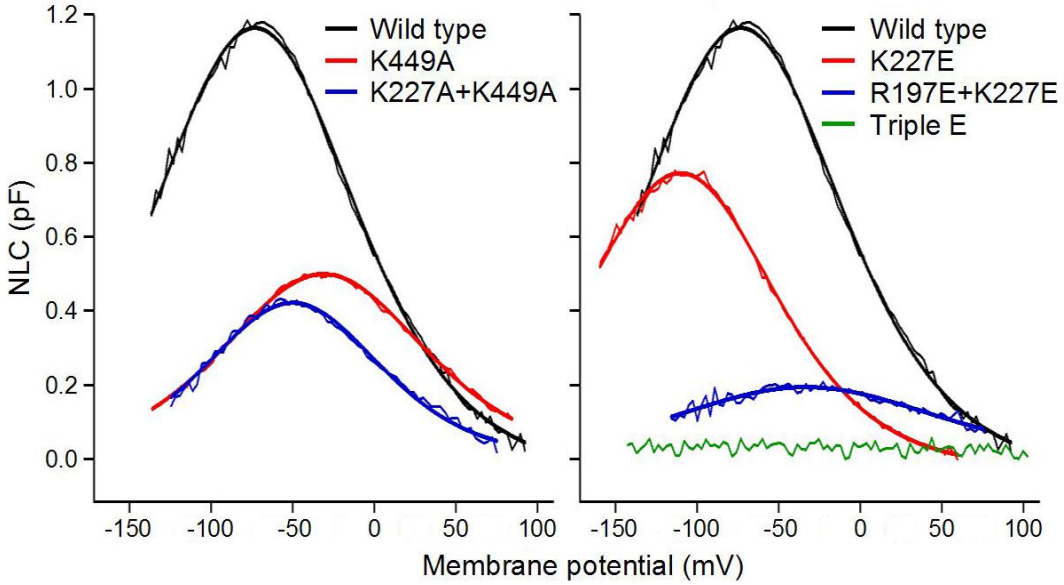

Figure 4-4. NLC obtained from HEK cells transfected with Ala and Glu substitutions. ***A.*** Representative capacitance-voltage curves of K449A and K227A+K449A. ***B.*** Representative capacitance-voltage curves of K227E, R197E+K227E and triple E.

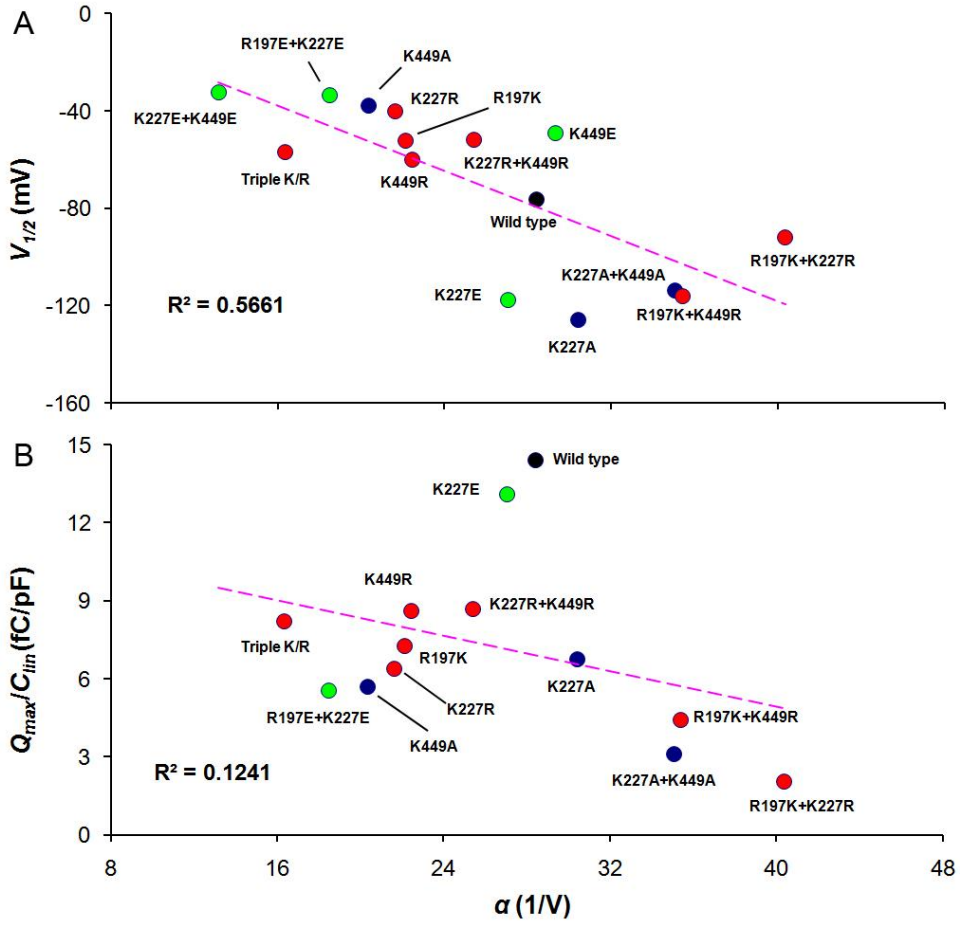

Figure 4-5. Relevance of $V_{1/2}$ / Q_{max} and α. Three different series of mutants are shown in different colors, positive in red, neutral in blue and negative in green. Wild type gPres is shown in black. The pooled data showed a negative correlation between $V_{1/2}$ and α (***A***) and no positive correlation between Q_{max}/C_{lin} and α (***B***).

IV. DISCUSSION

These studies contribute to the understanding of the structure and function of prestin in three ways. First, through the mutual substitution of Arg and Lys at the three sites, it is demonstrated for the first time that the size or charge location may play an important role in prestin function. Compared to Lys, Arg has a more bulky guanidinium group protrusion in which the orientation of the charges also differs. The differences between these two amino acids are about 23 Å in size and about 3 Å in charge location of the side chain (Fig. 4-3, the insert), while such tiny differences on the side chain caused major alterations in voltage sensing of prestin. The alteration in NLC included not only the total charge movement, but also the peak voltage and the slope factor (Table 4-3). Whether the size or the charge location governs the difference in NLC as a result of these mutations is not clear yet, but the size of the side chain is reported to be essential in ion gating in another chloride transporter, ClC-ec1. Shortening the side chains of the amino acids on the two gating residues abolishes the gating properties and eliminates the substrate binding sites, and thus confers the transporter with channel-like properties (Jayaram et al. 2008).

By studying the double and triple mutations, it is found that multiple sites may be involved in voltage sensing of prestin, and have a cumulative effect. Mutations on each of the three sites had a significant influence on NLC, while double and triple mutations

showed more diminished NLC than those with single mutations. This may partly explain why single mutations on positively charged amino acids did not abolish NLC in previous studies (Oliver et al. 2001). The difference in the membrane-associated expression level among the mutations does not seem to be enough to account for this trend for two reasons: 1. The amplitude of NLC in most constructs decreased to about or less than one half of that of the wild type, regardless their membrane expression level (Table 4-3 and Figs 4-2, 4-3, 4-4). 2. All of the positive mutations had good membrane-associated fluorescence expression while the NLC of the triple positive mutation was small. On the other hand, the expression level of R197E+K227E was weak while its NLC was higher than that of some other constructs (Table 4-2 and Figs 4-2, 4-4).

Finally, correlation analysis of the group data may indicate how these mutations influence the voltage-dependence of prestin. The slope factor α is the key parameter for it is related to both the valence z and membrane dielectric δ. A previous assumption is that the change of α is contributed by the 'apparent valence' z, which is defined as $z = q \times d$, where q is the elementary charge of the voltage sensor and d is its traveling distance in the membrane (Bai et al. 2009; Rybalchenko and Santos-Sacchi 2008). In this case there should be a positive relationship between Q_{max} and α because Q_{max} equals to the product of q and the number of prestin molecules, while there should have no relationship between $V_{1/2}$ and α. However, analysis of the present data revealed negative relationships between $V_{1/2}$ and α, and no positive relationship between Q_{max} and α, which means the valence z should not account for the change of voltage dependence of prestin in these mutations. Instead, the dielectric properties such as the damping or resistance of the tunnel may be altered in these mutations, because of the changes in size or charge of the R group. This, in turn, may facilitate or obstruct the movement of the anions in the

electrical field inside prestin molecule, and then influence the voltage operation range as well as the peak voltage. Further studies on electromotility of these mutants with a more precise device may give more evidence to support this possibility.

Interestingly, these three sites were tested previously in other studies, by substitution with neutral amino acid glutamine, which contains a polar side chain [R197Q in (Oliver et al. 2001); K227Q and K449Q in (Bai et al. 2009), respectively]. All of the mutants were expressed on cell surface. R197Q and K227Q showed left-shifted $V_{1/2}$ without significant changes in Q_{max} and α, similar to those of K227E. K449Q showed a decreased Q_{max} and α accompanied by right-shifted $V_{1/2}$, similar to those of K449A. These results showed influences on NLC that were consistent with the correlation analysis reported here.

CHAPTER 5: SUMMERIZATION AND FUTURE STUDIES

I. SUMMERIZATION OF THE RESULTS AND CONCLUSIONS

A. Prestin evolves from anion transporter

SLC26A is a highly versatile transporter family involved in the exchange of monovalent and divalent anions such as chloride, sulfate, iodide, formate, oxalate, hydroxyl ion and bicarbonate (Jiang et al. 2002; Karniski et al. 1998; Scott and Karniski 2000). The members in this family participate in various physiological processes such as skeletal development (Hastbacka et al. 1994), synthesis of thyroid hormone (Everett et al. 1997), regulation of intracellular pH in the duodenum (Simpson et al. 2010) and Na^+-Cl^- exchange in the renal proximal tubule (Knauf et al. 2001). NMV SLC26A5 also maintains transporter function (Albert et al. 2007; Schaechinger and Oliver 2007) while mammalian SLC26A5 (prestin) is unique for its motility (Zheng et al. 2000). All of these studies suggest that mammalian prestin evolved from anion transporter and the gain of motor function is a recent evolutionary event. When this transition occurred and what molecular innovation is acquired in prestin sequence which gives rise to the generation of motor function, however, remain unsolved. Through the comparison of mammalian and NMV prestins, these studies provide direct evidence that this transition has already occurred in prototherian (Fig 2-1) and corresponds with the evolution of the mammalian Organ of Corti and OHC. Moreover, this gain of motor function appears to be accompanied by a decrease in transporter function. The transport capability of prestin apparently decreases gradually as the NLC (signature of motility) increases and is minimized in mammals with motile capability (Fig 2-3). Although it is suggested that mammalian prestin still retains transport function (Bai et al. 2009; Muallem and Ashmore

2006), results of the current study suggest that even if residual transport capability is retained, the contribution of mammalian prestin to anion transport is minimum (Figs 2-4 and 2-5).

The connections between the motor and anion transporters have critical implications on the structure and function of prestin. Mammalian prestin sequence shares a similar hydrophobicity to those of its NMV ancestors (Albert et al. 2007; Schaechinger and Oliver 2007), suggesting a similar spatial configuration of the two homologous molecules. The piezoelectric property associated with the motility of prestin also resembles the bi-directional ion movement through transporters. Presumably, prestin can move in a frequency as high as tens of KHz, the same range as the turnover rate of transporters (Accardi et al. 2004; Walden et al. 2007). These connections strongly indicate that prestin also shares a similar structure and working mechanism with transporters. Although the crystalographic structure for prestin is yet to be elucidated, these studies suggest that the molecular motif for transporter and motility foundations are distinct. This, provides new ways to further understand the one-of-a-kind motor function of prestin.

B. The meEM motif is critical for the gain of motor function

It is theorized that prestin comprises at least two functional regions: the voltage sensor and the actuator (Dallos and Fakler 2002), both of which are assumed to be newly derived features in mammalian prestin. Attempts to identify the critical motile regions have not yet identified the protein motif, the reason for this may be due to the entirely new working mechanism of prestin [ATP independent (Holley and Ashmore 1988) and its function as a membrane motor (Kalinec et al. 1992)] which has no structural or sequential relative to date. Recently, unique conservative sites or motifs in mammalian prestin were identified through the comparison of prestin paralogs and orthologs from

mammalian and NMV species (Okoruwa et al. 2008). These sites or motifs distribute over the whole SulpTP core and presumably contain elements essential for the newly derived motor function of mammalian prestin. Among these regions, the 11-amino acid meEM motif in EL2 of prestin 12 TMD model is extremely significant, for it exhibits a high degree of diversification in NMV orthologs, which is potentially fixed by positive selection (Elgoyhen and Franchini 2010). This amino acid stretch is shorter in length than those of NMV orthologs (Okoruwa et al. 2008). In this study, the introduction of this meEM motif into NMV prestin confers the transporter with motility capability (Figs 3-3, 3-4 and 3-5), which strongly suggests its critical role in the transition of anion transporter to motor protein.

The mechanism underlying this transporter to motor transition is not clear yet. The interesting thing is the location of the critical meEM motif. It was shown, for the first time, that a hydrophilic loop instead of a helix region was important for this gain of function. Relating to this, recent studies suggest that transporters share a common structure, with an outer shell surrounding an inner core which is the motile unit of the transporter (refer to Chapter 1, III C). Based on unpublished data from Lovas and Beisel (Creighton University), prestin may share such a spatial configuration. This suggests that the potential motility of the molecule has existed. What evolution needed to do was just transferring this fast movement of the inner core to the whole molecule. Although further studies are needed for the details, it is reasonable to assume that the remarkable motility of prestin is no more than a conformational change in the inner motile unit of transporter *per se*. The movement of the inner core might have been transferred to the outer shell somehow in mammalian prestin, as the consequence of the shortening of the loop connecting these two parts.

C. The size of the tunnel is critical for prestin function.

The critical role of the size of the side chain in ion gating of transporters was reported previously (Jayaram et al. 2008), and results from this study on the three positive amino acids extend this observation to prestin, the new type of motor protein (Table 4-3 and Fig 4-3). Due to the incompletion of the putative tunnel, the movement of Cl^- in prestin is displayed as NLC. Altered ion movement is postulated to change the parameters of NLC. While Q_{max}, the total charge movement, is likely to be influenced by the membrane-associated expression level (Kumano et al. 2009), the $V_{1/2}$ (peak voltage) and α (slope factor) should be independent of the expression level. Alterations in $V_{1/2}$ and α should thus reflect the changes in the function of prestin itself. Most of the mutations at the three sites showed significant changes on $V_{1/2}$ (Table 4-3), indicating the importance of the three positive amino acids in the voltage sensing of prestin, possibly by serving as the anion binding sites. Furthermore, the cumulative effects strongly suggested the participation of multiple sites in this process.

Through the analysis of the relationship between Q_{max} / $V_{1/2}$ and α, it is suggested that the dielectric properties may be important and responsible for the alteration of the voltage -dependence of prestin (Fig 4-5). The dielectric property of the tunnel region, manifesting as the damping or resistance of the tunnel, may be altered because of the changes on size of the R group of the consisting amino acids. Similar influence of the dielectric properties may also account for the shifting of NLC parameters under different anion environments (Rybalchenko and Santos-Sacchi 2008), for anions different in size should have different damping or resistance moving in the tunnel. Indeed, Rybalchenko and Santos-Sacchi (2008) also emphasized that the shift of NLC property is determined by the nature of anion itself. The alteration on dielectric properties in these mutations is more credible

than on tunnel length suggested by other studies (Bai et al. 2009; Rybalchenko and Santos-Sacchi 2008), for the mutations of single amino acids should not likely cause significant changes on the tunnel length.

II. FUTURE STUDIES

Considerable progress has been made on the appreciation of the merits of the unique motor protein prestin from current studies, by manifesting its functional evolution, identifying the essential sequence for the transition from a transporter to a motor protein, and speculating the mechanisms underlying its voltage dependence and motility. There are, however, still questions about the structure and function of prestin which have yet to be answered. For example, although the formate transport capability of mammalian prestin is minimal, the possibility that mammalian prestin can transport other anions across the membrane (Bai et al. 2009; Muallem and Ashmore 2006) cannot be completely ruled out. Presently, the three-dimensional structure of prestin is unresolved. Further studies based on the results of this project and the remaining questions are discussed below.

First, assessment of prestin's transport function using other anions may give us a comprehensive understanding of prestin function and resolve the disagreements in different studies (Bai et al. 2009; Muallem and Ashmore 2006; Schaechinger and Oliver 2007). Substrates of the SLC26A family such as sulfate, iodide, oxalate, hydroxyl ion and bicarbonate should be considered. The traditional radioisotope uptake technique used here and the electrophysiological method used in other studies (Schaechinger and Oliver 2007) may be applied. If mammalian prestin retains transport capabilities for certain anions, it may indicate its role in the maintenance of the extracellular or intracellular ion

environment of OHC, which is a totally new perspective for prestin function. In addition, studies including prestin orthologs from more species such as frog, lizard and opossum might yield more details regarding the functional evolution of prestin.

Second, further investigations can be done on the eleven amino acid segment to determine the structural alterations underlying the gain of motor function. Step-wise substitution of the eleven amino acid segment might further identify specific amino acids essential for the transporter-motor transition of prestin. For example, mutations on the prolyl and glycyl residues in the meEM motif might facilitate the formation of the α-helix in this region and thus alter its secondary structure. Expansion of segment size may also provide additional insights. Additionally, if prestin really shares the rocker-switch structure of the transporter (refer to Chapter 1, III C), the shortening or elongation of this meEM motif is possibly related to the transfer of the movement from the inner transport machinery to the outer cylinder, which is seen in other transporters. Functional studies on these mutations might give more implications on the structure and working mechanism of prestin.

Third, the combination of further computational modeling, comparative genomic and functional studies might identify other functionally critical regions on prestin sequence. For example, the gating elements of the transporters are often amino acids with hydroxyl group, such as Serine or Tryptophan (Jayaram et al. 2008). Modeling studies and comparison of prestin sequence with known structures of transporters might identify candidates of the gating elements of prestin molecule. Studies of the mutations on these sites testing their relevant functional changes should therefore determine their role in ion gating or the generation of the NLC of prestin.

Fourth, transgenic animal models could be used for the eventual verification of the gain of motor function of prestin. By introducing chimera Zf(g) or Ck(g) into prestin knock-out mice, the expression, coupling of the chimera prestin with the scaffold of the cytoskeleton of OHC, and hearing restoration of the animals can be tested. More interestingly, introducing Ck(g) into chicken inner ear might confer motility and NLC to nonmammalian vertebrates hair cells, and might thus generate a chicken with "super hearing".

Finally, application of advanced and improved techniques is also needed for further understanding of prestin structure and function. With the application of more precise motility-measuring systems or methods, the quantitative comparison of the motor function of prestin orthologs might be better investigated. This might provide clues on how the motor function of prestin evolved and underwent fixation in mammals. The purification of prestin and its reconstitution into the artificial lipid bilayer might allow the direct observation of prestin structure using biological techniques such as atomic force microscopy, and might enable functional measurement in a "clean" membrane environment (Kumano et al. 2010). Tryptophan or cysteine-scanning mutagenesis combined with voltage-clamp fluorimetry might also be used to directly detect the movement of the motor region or the conformational change of the molecule (McGuire et al. 2010). Most of all, crystallography data is an absolute requirement for the elucidation of protein structure, and new ways to maximize prestin protein yield in a expression system must be discovered before the molecular basis of prestin movement can really be elucidated.

REFERENCES

Abe T, Kakehata S, Kitani R, Maruya S, Navaratnam D, Santos-Sacchi J, and Shinkawa H. Developmental expression of the outer hair cell motor prestin in the mouse. *J Membr Biol* 215: 49-56, 2007.

Accardi A, Kolmakova-Partensky L, Williams C, and Miller C. Ionic currents mediated by a prokaryotic homologue of CLC Cl- channels. *J Gen Physiol* 123: 109-119, 2004.

Albert JT, Winter H, Schaechinger TJ, Weber T, Wang X, He DZ, Hendrich O, Geisler HS, Zimmermann U, Oelmann K, Knipper M, Gopfert MC, and Oliver D. Voltage-sensitive prestin orthologue expressed in zebrafish hair cells. *J Physiol* 580: 451-461, 2007.

Ashmore J. Cochlear outer hair cell motility. *Physiol Rev* 88: 173-210, 2008.

Ashmore JF. A fast motile response in guinea-pig outer hair cells: the cellular basis of the cochlear amplifier. *J Physiol* 388: 323-347, 1987.

Ashmore JF. Transducer motor coupling in cochear outer hair cells. In: *Cochlear Mechanisms*, edited by Wilson JP, and Kemp DT. New York: Plenum Press, 1989, p. 107-114.

Bai JP, Surguchev A, Montoya S, Aronson PS, Santos-Sacchi J, and Navaratnam D. Prestin's anion transport and voltage-sensing capabilities are independent. *Biophys J* 96: 3179-3186, 2009.

Bekesy G. Experiments in Hearing. *New York: McGraw-Hill* 1960.

Belyantseva IA, Adler HJ, Curi R, Frolenkov GI, and Kachar B. Expression and localization of prestin and the sugar transporter GLUT-5 during development of electromotility in cochlear outer hair cells. *J Neurosci* 20: RC116, 2000.

Brownell WE, Bader CR, Bertrand D, and de Ribaupierre Y. Evoked mechanical responses of isolated cochlear outer hair cells. *Science* 227: 194-196, 1985.

Chan DK, and Hudspeth AJ. Ca2+ current-driven nonlinear amplification by the mammalian cochlea in vitro. *Nat Neurosci* 8: 149-155, 2005.

Crawford AC, and Fettiplace R. The mechanical properties of ciliary bundles of turtle cochlear hair cells. *J Physiol* 364: 359-379, 1985.

Dallos P. Cochlear amplification, outer hair cells and prestin. *Curr Opin Neurobiol* 18: 370-376, 2008.

Dallos P, and Evans BN. High-frequency motility of outer hair cells and the cochlear amplifier. *Science* 267: 2006-2009, 1995.

Dallos P, and Fakler B. Prestin, a new type of motor protein. *Nat Rev Mol Cell Biol* 3: 104-111, 2002.

Dallos P, Wu X, Cheatham MA, Gao J, Zheng J, Anderson CT, Jia S, Wang X, Cheng WH, Sengupta S, He DZ, and Zuo J. Prestin-based outer hair cell motility is necessary for mammalian cochlear amplification. *Neuron* 58: 333-339, 2008.

Davis H. A model for transducer action in the cochlea. *Cold Spring Harb Symp Quant Biol* 30: 181-190, 1965.

Davis H, Deatherage BH, Rosenblut B, Fernandez C, Kimura R, and Smith CA. Modification of cochlear potentials produced by streptomycin poisoning and by extensive venous obstruction. *Laryngoscope* 68: 596-627, 1958.

Deak L, Zheng J, Orem A, Du GG, Aguinaga S, Matsuda K, and Dallos P. Effects of cyclic nucleotides on the function of prestin. *J Physiol* 563: 483-496, 2005.

Diallinas G. Biochemistry. An almost-complete movie. *Science* 322: 1644-1645, 2008.

Dong XX, Ospeck M, and Iwasa KH. Piezoelectric reciprocal relationship of the membrane motor in the cochlear outer hair cell. *Biophys J* 82: 1254-1259, 2002.

Dorwart MR, Shcheynikov N, Yang D, and Muallem S. The solute carrier 26 family of proteins in epithelial ion transport. *Physiology (Bethesda)* 23: 104-114, 2008.

Dossena S, Rodighiero S, Vezzoli V, Nofziger C, Salvioni E, Boccazzi M, Grabmayer E, Botta G, Meyer G, Fugazzola L, Beck-Peccoz P, and Paulmichl M. Functional characterization of wild-type and mutated pendrin (SLC26A4), the anion transporter involved in Pendred syndrome. *J Mol Endocrinol* 43: 93-103, 2009.

Elgoyhen AB, and Franchini LF. Prestin and the cholinergic receptor of hair cells: Positively-selected proteins in mammals. *Hear Res* 2010.

Evans BN, Hallworth R, and Dallos P. Outer hair cell electromotility: the sensitivity and vulnerability of the DC component. *Hear Res* 52: 288-304, 1991.

Everett LA, Glaser B, Beck JC, Idol JR, Buchs A, Heyman M, Adawi F, Hazani E, Nassir E, Baxevanis AD, Sheffield VC, and Green ED. Pendred syndrome is caused by mutations in a putative sulphate transporter gene (PDS). *Nat Genet* 17: 411-422, 1997.

Faham S, Watanabe A, Besserer GM, Cascio D, Specht A, Hirayama BA, Wright EM, and Abramson J. The crystal structure of a sodium galactose transporter reveals mechanistic insights into Na+/sugar symport. *Science* 321: 810-814, 2008.

Fahlke C, Durr C, and George AL, Jr. Mechanism of ion permeation in skeletal muscle chloride channels. *J Gen Physiol* 110: 551-564, 1997.

Fernandez C, and Schmidt RS. The Opossum Ear and Evolution of the Coiled Cochlea. *J Comp Neurol* 121: 151-159, 1963.

Franchini LF, and Elgoyhen AB. Adaptive evolution in mammalian proteins involved in cochlear outer hair cell electromotility. *Mol Phylogenet Evol* 41: 622-635, 2006.

Frank G, Hemmert W, and Gummer AW. Limiting dynamics of high-frequency electromechanical transduction of outer hair cells. *Proc Natl Acad Sci U S A* 96: 4420-4425, 1999.

Gale JE, and Ashmore JF. Charge displacement induced by rapid stretch in the basolateral membrane of the guinea-pig outer hair cell. *Proc Biol Sci* 255: 243-249, 1994.

Gale JE, and Ashmore JF. An intrinsic frequency limit to the cochlear amplifier. *Nature* 389: 63-66, 1997.

Gao J, Wang X, Wu X, Aguinaga S, Huynh K, Jia S, Matsuda K, Patel M, Zheng J, Cheatham M, He DZ, Dallos P, and Zuo J. Prestin-based outer hair cell electromotility in knockin mice does not appear to adjust the operating point of a cilia-based amplifier. *Proc Natl Acad Sci U S A* 104: 12542-12547, 2007.

Gold T. Hearing. II. The physical basis of the action of the cochlea. *Proc R Soc Lond B Biol Sci* 135: 462-491, 1948.

Gold T, and Pumphrey RJ. Hearing. I. The cochlea as a frequency analyser. *Proc R Soc Lond B Biol Sci* 135: 162-491, 1948.

Gulley RL, and Reese TS. Freeze-fracture studies on the synapses in the organ of Corti. *J Comp Neurol* 171: 517-543, 1977.

Hallworth R, Evans BN, and Dallos P. The location and mechanism of electromotility in guinea pig outer hair cells. *J Neurophysiol* 70: 549-558, 1993.

Hastbacka J, de la Chapelle A, Kaitila I, Sistonen P, Weaver A, and Lander E. Linkage disequilibrium mapping in isolated founder populations: diastrophic dysplasia in Finland. *Nat Genet* 2: 204-211, 1992.

Hastbacka J, de la Chapelle A, Mahtani MM, Clines G, Reeve-Daly MP, Daly M, Hamilton BA, Kusumi K, Trivedi B, Weaver A, and et al. The diastrophic dysplasia gene

encodes a novel sulfate transporter: positional cloning by fine-structure linkage disequilibrium mapping. *Cell* 78: 1073-1087, 1994.

He DZ, Beisel KW, Chen L, Ding DL, Jia S, Fritzsch B, and Salvi R. Chick hair cells do not exhibit voltage-dependent somatic motility. *J Physiol* 546: 511-520, 2003.

He DZ, Evans BN, and Dallos P. First appearance and development of electromotility in neonatal gerbil outer hair cells. *Hear Res* 78: 77-90, 1994.

He DZ, Jia S, Sato T, Zuo J, Andrade LR, Riordan GP, and Kachar B. Changes in plasma membrane structure and electromotile properties in prestin deficient outer hair cells. *Cytoskeleton (Hoboken)* 67: 43-55, 2010.

He DZ, Zheng J, Kalinec F, Kakehata S, and Santos-Sacchi J. Tuning in to the amazing outer hair cell: membrane wizardry with a twist and shout. *J Membr Biol* 209: 119-134, 2006.

Hoglund P, Haila S, Scherer SW, Tsui LC, Green ED, Weissenbach J, Holmberg C, de la Chapelle A, and Kere J. Positional candidate genes for congenital chloride diarrhea suggested by high-resolution physical mapping in chromosome region 7q31. *Genome Res* 6: 202-210, 1996.

Holley MC, and Ashmore JF. A cytoskeletal spring in cochlear outer hair cells. *Nature* 335: 635-637, 1988.

Holt JR, and Corey DP. Two mechanisms for transducer adaptation in vertebrate hair cells. *Proc Natl Acad Sci U S A* 97: 11730-11735, 2000.

Huang G, and Santos-Sacchi J. Mapping the distribution of the outer hair cell motility voltage sensor by electrical amputation. *Biophys J* 65: 2228-2236, 1993.

Huang G, and Santos-Sacchi J. Motility voltage sensor of the outer hair cell resides within the lateral plasma membrane. *Proc Natl Acad Sci U S A* 91: 12268-12272, 1994.

Hudspeth A. Mechanical amplification of stimuli by hair cells. *Curr Opin Neurobiol* 7: 480-486, 1997.

Hudspeth AJ. Making an effort to listen: mechanical amplification in the ear. *Neuron* 59: 530-545, 2008.

Hudspeth AJ, Choe Y, Mehta AD, and Martin P. Putting ion channels to work: mechanoelectrical transduction, adaptation, and amplification by hair cells. *Proc Natl Acad Sci U S A* 97: 11765-11772, 2000.

Iwasa KH. A membrane motor model for the fast motility of the outer hair cell. *J Acoust Soc Am* 96: 2216-2224, 1994.

Iwasa KH. A two-state piezoelectric model for outer hair cell motility. *Biophys J* 81: 2495-2506, 2001.

Jayaram H, Accardi A, Wu F, Williams C, and Miller C. Ion permeation through a Cl--selective channel designed from a CLC Cl-/H+ exchanger. *Proc Natl Acad Sci U S A* 105: 11194-11199, 2008.

Jia S, and He DZ. Motility-associated hair-bundle motion in mammalian outer hair cells. *Nat Neurosci* 8: 1028-1034, 2005.

Jiang Z, Grichtchenko, II, Boron WF, and Aronson PS. Specificity of anion exchange mediated by mouse Slc26a6. *J Biol Chem* 277: 33963-33967, 2002.

Kalinec F, Holley MC, Iwasa KH, Lim DJ, and Kachar B. A membrane-based force generation mechanism in auditory sensory cells. *Proc Natl Acad Sci U S A* 89: 8671-8675, 1992.

Karniski LP, Lotscher M, Fucentese M, Hilfiker H, Biber J, and Murer H. Immunolocalization of sat-1 sulfate/oxalate/bicarbonate anion exchanger in the rat kidney. *Am J Physiol* 275: F79-87, 1998.

Kemp DT. Stimulated acoustic emissions from within the human auditory system. *J Acoust Soc Am* 64: 1386-1391, 1978.

Kennedy HJ, Crawford AC, and Fettiplace R. Force generation by mammalian hair bundles supports a role in cochlear amplification. *Nature* 433: 880-883, 2005.

Kennedy HJ, Evans MG, Crawford AC, and Fettiplace R. Fast adaptation of mechanoelectrical transducer channels in mammalian cochlear hair cells. *Nat Neurosci* 6: 832-836, 2003.

Kim DO. Active and nonlinear cochlear biomechanics and the role of outer-hair-cell subsystem in the mammalian auditory system. *Hear Res* 22: 105-114, 1986.

Knauf F, Yang CL, Thomson RB, Mentone SA, Giebisch G, and Aronson PS. Identification of a chloride-formate exchanger expressed on the brush border membrane of renal proximal tubule cells. *Proc Natl Acad Sci U S A* 98: 9425-9430, 2001.

Kumano S, Murakoshi M, Iida K, Hamana H, and Wada H. Atomic force microscopy imaging of the structure of the motor protein prestin reconstituted into an artificial lipid bilayer. *FEBS Lett* 584: 2872-2876, 2010.

Kumano S, Tan X, He DZ, Iida K, Murakoshi M, and Wada H. Mutation-induced reinforcement of prestin-expressing cells. *Biochem Biophys Res Commun* 389: 569-574, 2009.

Ladhams A, and Pickles JO. Morphology of the monotreme organ of Corti and macula lagena. *J Comp Neurol* 366: 335-347, 1996.

Li G, Wang J, Rossiter SJ, Jones G, Cotton JA, and Zhang S. The hearing gene Prestin reunites echolocating bats. *Proc Natl Acad Sci U S A* 105: 13959-13964, 2008.

Li Y, Liu Z, Shi P, and Zhang J. The hearing gene Prestin unites echolocating bats and whales. *Curr Biol* 20: R55-56, 2010.

Liberman MC, Gao J, He DZ, Wu X, Jia S, and Zuo J. Prestin is required for electromotility of the outer hair cell and for the cochlear amplifier. *Nature* 419: 300-304, 2002.

Ludwig J, Oliver D, Frank G, Klocker N, Gummer AW, and Fakler B. Reciprocal electromechanical properties of rat prestin: the motor molecule from rat outer hair cells. *Proc Natl Acad Sci U S A* 98: 4178-4183, 2001.

Manley GA. Cochlear mechanisms from a phylogenetic viewpoint. *Proc Natl Acad Sci U S A* 97: 11736-11743, 2000.

Manley GA, Kirk DL, Koppl C, and Yates GK. In vivo evidence for a cochlear amplifier in the hair-cell bundle of lizards. *Proc Natl Acad Sci U S A* 98: 2826-2831, 2001.

Matei VA, Feng F, Pauley S, Beisel KW, Nichols MG, and Fritzsch B. Near-infrared laser illumination transforms the fluorescence absorbing X-Gal reaction product BCI into a transparent, yet brightly fluorescent substance. *Brain Res Bull* 70: 33-43, 2006.

McGuire RM, Liu H, Pereira FA, and Raphael RM. Cysteine mutagenesis reveals transmembrane residues associated with charge translocation in prestin. *J Biol Chem* 285: 3103-3113, 2010.

Mount DB, and Romero MF. The SLC26 gene family of multifunctional anion exchangers. *Pflugers Arch* 447: 710-721, 2004.

Muallem D, and Ashmore J. An anion antiporter model of prestin, the outer hair cell motor protein. *Biophys J* 90: 4035-4045, 2006.

Navaratnam D, Bai JP, Samaranayake H, and Santos-Sacchi J. N-terminal-mediated homomultimerization of prestin, the outer hair cell motor protein. *Biophys J* 89: 3345-3352, 2005.

Navarrete EG, and Santos-Sacchi J. On the effect of prestin on the electrical breakdown of cell membranes. *Biophys J* 90: 967-974, 2006.

Okoruwa OE, Weston MD, Sanjeevi DC, Millemon AR, Fritzsch B, Hallworth R, and Beisel KW. Evolutionary insights into the unique electromotility motor of mammalian outer hair cells. *Evol Dev* 10: 300-315, 2008.

Oliver D, He DZ, Klocker N, Ludwig J, Schulte U, Waldegger S, Ruppersberg JP, Dallos P, and Fakler B. Intracellular anions as the voltage sensor of prestin, the outer hair cell motor protein. *Science* 292: 2340-2343, 2001.

Pasqualetto E, Aiello R, Gesiot L, Bonetto G, Bellanda M, and Battistutta R. Structure of the cytosolic portion of the motor protein prestin and functional role of the STAS domain in SLC26/SulP anion transporters. *J Mol Biol* 400: 448-462, 2010.

Pickles JO. An introduction to the physiology of hearing (third edition). *Emerald Group Publishing Limited* 25-32, 2008.

Rajagopalan L, Patel N, Madabushi S, Goddard JA, Anjan V, Lin F, Shope C, Farrell B, Lichtarge O, Davidson AL, Brownell WE, and Pereira FA. Essential helix interactions in the anion transporter domain of prestin revealed by evolutionary trace analysis. *J Neurosci* 26: 12727-12734, 2006.

Ricci AJ, Wu YC, and Fettiplace R. The endogenous calcium buffer and the time course of transducer adaptation in auditory hair cells. *J Neurosci* 18: 8261-8277, 1998.

Robles L, and Ruggero MA. Mechanics of the mammalian cochlea. *Physiol Rev* 81: 1305-1352, 2001.

Russell IJ, Cody AR, and Richardson GP. The responses of inner and outer hair cells in the basal turn of the guinea-pig cochlea and in the mouse cochlea grown in vitro. *Hear Res* 22: 199-216, 1986.

Rybalchenko V, and Santos-Sacchi J. Anion control of voltage sensing by the motor protein prestin in outer hair cells. *Biophys J* 95: 4439-4447, 2008.

Santos-Sacchi J. Asymmetry in voltage-dependent movements of isolated outer hair cells from the organ of Corti. *J Neurosci* 9: 2954-2962, 1989.

Santos-Sacchi J. Reversible inhibition of voltage-dependent outer hair cell motility and capacitance. *J Neurosci* 11: 3096-3110, 1991.

Santos-Sacchi J, Shen W, Zheng J, and Dallos P. Effects of membrane potential and tension on prestin, the outer hair cell lateral membrane motor protein. *J Physiol* 531: 661-666, 2001.

Schaechinger TJ, and Oliver D. Nonmammalian orthologs of prestin (SLC26A5) are electrogenic divalent/chloride anion exchangers. *Proc Natl Acad Sci U S A* 104: 7693-7698, 2007.

Schweinfest CW, Henderson KW, Suster S, Kondoh N, and Papas TS. Identification of a colon mucosa gene that is down-regulated in colon adenomas and adenocarcinomas. *Proc Natl Acad Sci U S A* 90: 4166-4170, 1993.

Scott DA, and Karniski LP. Human pendrin expressed in Xenopus laevis oocytes mediates chloride/formate exchange. *Am J Physiol Cell Physiol* 278: C207-211, 2000.

Sellick PM, Patuzzi R, and Johnstone BM. Measurement of basilar membrane motion in the guinea pig using the Mossbauer technique. *J Acoust Soc Am* 72: 131-141, 1982.

Simpson JE, Walker NM, Supuran CT, Soleimani M, and Clarke LL. Putative anion transporter-1 (Pat-1, Slc26a6) contributes to intracellular pH regulation during H+-dipeptide transport in duodenal villous epithelium. *Am J Physiol Gastrointest Liver Physiol* 298: G683-691, 2010.

Singh SK, Piscitelli CL, Yamashita A, and Gouaux E. A competitive inhibitor traps LeuT in an open-to-out conformation. *Science* 322: 1655-1661, 2008.

Tan X, Pecka JL, Okoruwa OE, Tang J, Zhang Q, Beisel KW, and He DZZ. From zebrafish to mammal: evolution of prestin, the motor protein of cochlear hair cells. *J Neurophysiol (submitted)* 2010a.

Tan X, Pecka JL, Okoruwa OE, Tang J, Zhang Q, Beisel KW, and He DZZ. From zebrafish to mammal: functional evolution of prestin, the motor protein of cochlear hair cells. *J Neurophysiol (submitted)* 2010b.

Walden M, Accardi A, Wu F, Xu C, Williams C, and Miller C. Uncoupling and turnover in a Cl-/H+ exchange transporter. *J Gen Physiol* 129: 317-329, 2007.

Wang X, Yang S, Jia S, and He DZZ. Prestin forms oligomer with four mechanically independent subunits. *Brain Res* (in press): 2010.

Weber T, Gopfert MC, Winter H, Zimmermann U, Kohler H, Meier A, Hendrich O, Rohbock K, Robert D, and Knipper M. Expression of prestin-homologous solute carrier (SLC26) in auditory organs of nonmammalian vertebrates and insects. *Proc Natl Acad Sci U S A* 100: 7690-7695, 2003.

Weyand S, Shimamura T, Yajima S, Suzuki S, Mirza O, Krusong K, Carpenter EP, Rutherford NG, Hadden JM, O'Reilly J, Ma P, Saidijam M, Patching SG, Hope RJ, Norbertczak HT, Roach PC, Iwata S, Henderson PJ, and Cameron AD. Structure and molecular mechanism of a nucleobase-cation-symport-1 family transporter. *Science* 322: 709-713, 2008.

Xue S, Mountain DC, and Hubbard AE. Electrically evoked basilar membrane motion. *J Acoust Soc Am* 97: 3030-3041, 1995.

Yamashita A, Singh SK, Kawate T, Jin Y, and Gouaux E. Crystal structure of a bacterial homologue of Na+/Cl--dependent neurotransmitter transporters. *Nature* 437: 215-223, 2005.

Zheng J, Du GG, Anderson CT, Keller JP, Orem A, Dallos P, and Cheatham M. Analysis of the oligomeric structure of the motor protein prestin. *J Biol Chem* 281: 19916-19924, 2006.

Zheng J, Du GG, Matsuda K, Orem A, Aguinaga S, Deak L, Navarrete E, Madison LD, and Dallos P. The C-terminus of prestin influences nonlinear capacitance and plasma membrane targeting. *J Cell Sci* 118: 2987-2996, 2005.

Zheng J, Long KB, Shen W, Madison LD, and Dallos P. Prestin topology: localization of protein epitopes in relation to the plasma membrane. *Neuroreport* 12: 1929-1935, 2001.

Zheng J, Madison LD, Oliver D, Fakler B, and Dallos P. Prestin, the motor protein of outer hair cells. *Audiol Neurootol* 7: 9-12, 2002.

Zheng J, Shen W, He DZ, Long KB, Madison LD, and Dallos P. Prestin is the motor protein of cochlear outer hair cells. *Nature* 405: 149-155, 2000.